Downloaded from jmg.bmj.com on February 14, 2012 - Published by group.bmj.com

Sequencher software (Gene Codes Corporation, Ann Arbor, Michigan, USA).

RESULTS AND DISCUSSION

Coverage analysis showed that 78.9% of all the X chromosome transcripts were completely covered by reads, and that 11.6% of transcripts were at least 90% covered. Almost all (99%) of these regions were covered by 20 reads or more (100 reads or more in 97%) by only single-lane sequencing. SNP genotyping was able to delineate the minimal linked region from rs763739 to rs1073455 (UCSC genome browser hg19 assembly, X chromosome coordinates: 76 804 990–126 844 262) (50 Mb). The maximum linked region was from rs1926354 to rs859587 (UCSC genome browser coordinates: 68 404 915–128 933 907) (60.5 Mb). Exome GAIIx sequencing with the two informatics methods identified four potentially interesting changes in the maximum linked region: c.1102AT (p.R368X) in *MCT8* (NM_006517; alternatively called *SLC16A2*); c.1402T→G (p.S468A) and c.1943A→G (p.H648R) in *CYLC1* (NM_021118); and c1606G→A (p.D536N) in *LRCH2* (NM_020871) (figure 1F). c.1102A→T (p.R368X) in *MCT8* was found heterozygously in the proband's healthy mother (II-3) and maternal grandmother (I-2), and hemizygously in the proband and his affected younger brother; each was confirmed by Sanger sequencing (figure 2). This change was not present among 92 normal female controls (0/184 alleles).

The *MCT8* gene encodes a thyroid hormone transporter and is implicated in syndromic X-linked mental retardation, Allan–Herndon–Dudley syndrome and Pelizaeus–Merzbacher-like disease (PMLD).[9–12] This nonsense mutation, c.1102A→T (p.R368X), which might lead to nonsense-mediated decay resulting in no protein production, is highly likely to be pathological. Based on the human gene mutation database (http://www.hgmd.cf.ac.uk/ac/index.php), three nonsense mutations in this gene have been previously registered: p.R245X, p.Q335X and p.S448X. The other identified variants, in *CYLC1* and *LRCH2*, are all SNPs because they were identified in normal controls: c.1402T→G (*CYLC1*): 5/182 alleles, c.1943A→G (*CYLC1*): 12/184 alleles and c1606G→A (*LRCH2*): 5/184 alleles. We concluded that the *MCT8* mutation was pathogenic in this family.

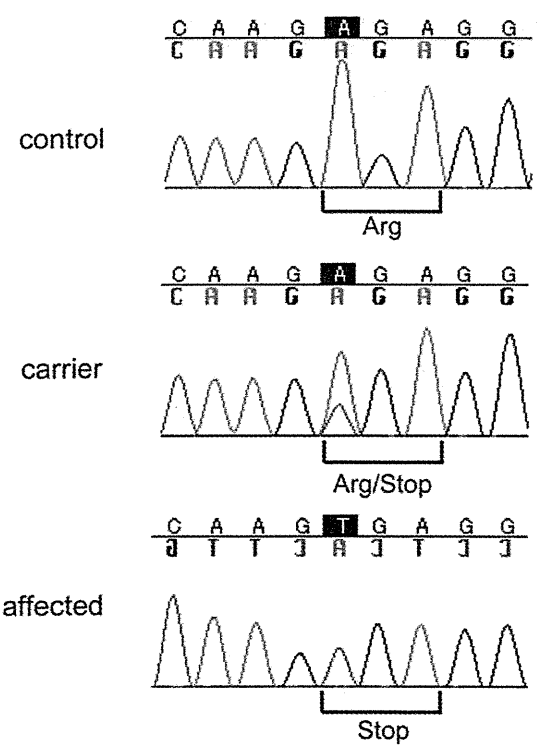

Figure 2 Electropherograms of a normal control, a carrier (mother) and the affected proband.

PMLD caused by *MCT8* mutations presents with infantile hypotonia, severe psychomotor development, nystagmus, generalised muscle weakness, dystopia, joint contracture and progressive spastic paraplegia. All affected male subjects develop the disease, while heterozygous female subjects are clinically normal or sometimes show mild thyroid dysfunction.[9 12] Brain MRI shows delayed myelination in the first few years of life, which subsequently improves but with residual neurological disability. The unique diagnostic feature of the disease is an abnormal thyroid hormone profile: increased free T_3, decreased free T_4 and normal thyroid-stimulating hormone.[12] The cases we analysed here showed clinical features and brain MRI findings typical of PMLD, but no thyroid hormone abnormalities. Based on regular laboratory testing and conventional PCR-based gene screening, we might have failed, or taken much longer, to identify the causative mutation. Thus, unbiased screening without prior knowledge is one of the advantages of NGS.

Thyroid hormone (T_4 and T_3) is important in neuronal development and its deficiency in the pre/neonatal stage causes a form of mental retardation called cretinism. T_4 is released from the thyroid as a prohormone and is altered to biologically active T_3 by iodothyronine deiodinases.[13] Active T_3 is delivered to the peripheral organs via thyroid hormone transporters. MCT8 is a thyroid hormone-specific transporter and is mainly expressed in the brain and liver.[14 15] In MCT8 deficiency, T_3 and T_4 uptake is impaired and deiodinase 2 is activated.[16] This results in increased serum T_3 levels because of T_3 accumulation in the peripheral blood. In previous reports, the majority of patients showed abnormal levels of thyroid hormones, but some displayed values within the normal range.[9 10 12 17 18] The variable range for abnormal thyroid hormone levels might be explained by unidentified modifier effect(s) and/or other transporter(s) that can compensate for MCT8 function.[19] Additionally, although MCT8 deficiency has been determined by abnormalities in thyroid function tests, it is unknown what proportion of the patients with MCT8 deficiency show abnormal thyroid function. We suggest that it is important to evaluate thyroid hormone function in PMLD with unknown cause.

Before the exome NGS analysis, we screened *PLP1*, *GJA12*, and seven other candidate genes mapped to the linked region: *MSN* (NM_002444), *IGBP1* (NM_001551), *SNX12* (NM_013346), *OGT* (NM_181672), *HDAC8* (NM_018486), *SH3BGRL* (NM_003022.2) and *PCDH11X* (NM_032967.2). Because we found no pathological changes, we adopted the exome sequencing strategy. We determined that exome sequencing with a single lane for each sample was sufficient to analyse all the transcripts of the X chromosome. In X-linked recessive diseases, male subjects are usually affected, and therefore the single X chromosome is the primary target of exome sequencing. Except for mosaic mutations, the hemizygous (rather than heterozygous) status of disease-related nucleotide changes is relatively easy to detect using all-or-none NGS reads (0% or 100% of reads). There was no difference in the ability of our two informatics methods (MAQ and NextGENe) to detect pathological changes. This approach could equally be applied to the analysis

Downloaded from jmg.bmj.com on February 14, 2012 - Published by group.bmj.com

of autosomal recessive diseases that manifest in the offspring of consanguineous relationships.

In conclusion, we rapidly identified a nonsense mutation in *MCT8* in a family with X-linked leucoencephalopathy using only a single lane of exome sequencing. This method is powerful for unbiased screening of disease-related mutations in X-linked or recessive conditions.

Acknowledgements We thank the family for their participation in this study.

Funding This work was supported by research grants from the Ministry of Health, Labour and Welfare (to HO, HSa, NMa and NMi), a grant-in-aid for scientific research from the Japan Society for the Promotion of Science (NMa), a grant-in-aid for young scientists from the Japan Society for the Promotion of Science (HSa), a grant from the 2010 Strategic Research Promotion of Yokohama City University (NMa), research grants from the Japan Epilepsy Research Foundation (HSa) and a research grant from the Naito Foundation (NMa). The study sponsors had no role in the study design; in the collection, analysis, and interpretation of the data; in the writing of the report; or in the decision to submit the paper for publication.

Competing interests None.

Patient consent Obtained.

Ethics approval This study was conducted with the approval of the institutional review board of Kanagawa Children's Medical Center and Yokohama City University School of Medicine.

Provenance and peer review Not commissioned; externally peer reviewed.

REFERENCES

1. **Shendure J,** Ji H. Next-generation DNA sequencing. *Nat Biotechnol* 2008;**26**:1135–45.
2. **Wheeler DA,** Srinivasan M, Egholm M, Shen Y, Chen L, McGuire A, He W, Chen YJ, Makhijani V, Roth GT, Gomes X, Tartaro K, Niazi F, Turcotte CL, Irzyk GP, Lupski JR, Chinault C, Song XZ, Liu Y, Yuan Y, Nazareth L, Qin X, Muzny DM, Margulies M, Weinstock GM, Gibbs RA, Rothberg JM. The complete genome of an individual by massively parallel DNA sequencing. *Nature* 2008;**452**:872–6.
3. **Ng SB,** Turner EH, Robertson PD, Flygare SD, Bigham AW, Lee C, Shaffer T, Wong M, Bhattacharjee A, Eichler EE, Bamshad M, Nickerson DA, Shendure J. Targeted capture and massively parallel sequencing of 12 human exomes. *Nature* 2009;**461**:272–6.
4. **Choi M,** Scholl UI, Ji W, Liu T, Tikhonova IR, Zumbo P, Nayir A, Bakkaloglu A, Ozen S, Sanjad S, Nelson-Williams C, Farhi A, Mane S, Lifton RP. Genetic diagnosis by whole exome capture and massively parallel DNA sequencing. *Proc Natl Acad Sci U S A* 2009;**106**:19096–101.
5. **Hodges E,** Xuan Z, Balija V, Kramer M, Molla MN, Smith SW, Middle CM, Rodesch MJ, Albert TJ, Hannon GJ, McCombie WR. Genome-wide in situ exon capture for selective resequencing. *Nat Genet* 2007;**39**:1522–7.
6. **Ng SB,** Buckingham KJ, Lee C, Bigham AW, Tabor HK, Dent KM, Huff CD, Shannon PT, Jabs EW, Nickerson DA, Shendure J, Bamshad MJ. Exome sequencing identifies the cause of a mendelian disorder. *Nat Genet* 2010;**42**:30–5.
7. **Nannya Y,** Sanada M, Nakazaki K, Hosoya N, Wang L, Hangaishi A, Kurokawa M, Chiba S, Bailey DK, Kennedy GC, Ogawa S. A robust algorithm for copy number detection using high-density oligonucleotide single nucleotide polymorphism genotyping arrays. *Cancer Res* 2005;**65**:6071–9.
8. **Li H,** Ruan J, Durbin R. Mapping short DNA sequencing reads and calling variants using mapping quality scores. *Genome Res* 2008;**18**:1851–8.
9. **Dumitrescu AM,** Liao XH, Best TB, Brockmann K, Refetoff S. A novel syndrome combining thyroid and neurological abnormalities is associated with mutations in a monocarboxylate transporter gene. *Am J Hum Genet* 2004;**74**:168–75.
10. **Friesema EC,** Grueters A, Biebermann H, Krude H, von Moers A, Reeser M, Barrett TG, Mancilla EE, Svensson J, Kester MH, Kuiper GG, Balkassmi S, Uitterlinden AG, Koehrle J, Rodien P, Halestrap AP, Visser TJ. Association between mutations in a thyroid hormone transporter and severe X-linked psychomotor retardation. *Lancet* 2004;**364**:1435–7.
11. **Frints SG,** Lenzner S, Bauters M, Jensen LR, Van Esch H, des Portes V, Moog U, Macville MV, van Roozendaal K, Schrander-Stumpel CT, Tzschach A, Marynen P, Fryns JP, Hamel B, van Bokhoven H, Chelly J, Beldjord C, Turner G, Gecz J, Moraine C, Raynaud M, Ropers HH, Froyen G, Kuss AW. *MCT8* mutation analysis and identification of the first female with Allan-Herndon-Dudley syndrome due to loss of *MCT8* expression. *Eur J Hum Genet* 2008;**16**:1029–37.
12. **Vaurs-Barriere C,** Deville M, Sarret C, Giraud G, Des Portes V, Prats-Vinas JM, De Michele G, Dan B, Brady AF, Boespflug-Tanguy O, Touraine R. Pelizaeus-Merzbacher-Like disease presentation of *MCT8* mutated male subjects. *Ann Neurol* 2009;**65**:114–18.
13. **Bianco AC,** Salvatore D, Gereben B, Berry MJ, Larsen PR. Biochemistry, cellular and molecular biology, and physiological roles of the iodothyronine selenodeiodinases. *Endocr Rev* 2002;**23**:38–89.
14. **Friesema EC,** Ganguly S, Abdalla A, Manning Fox J, Halestrap AP, Visser TJ. Identification of monocarboxylate transporter 8 as a specific thyroid hormone transporter. *J Biol Chem* 2003;**41**:40128–35.
15. **Lafreniere RG,** Carrel L, Willard HF. A novel transmembrane transporter encoded by the XPCT gene in Xq13.2. *Hum Mol Genet* 1994;**3**:1133–9.
16. **Dumitrescu AM,** Liao XH, Weiss RE, Millen K, Refetoff S. Tissue-specific thyroid hormone deprivation and excess in monocarboxylate transporter (mct) 8-deficient mice. *Endocrinology* 2006;**147**:4036–43.
17. **Maranduba CM,** Friesema EC, Kok F, Kester MH, Jansen J, Sertie AL, Passos-Bueno MR, Visser TJ. Decreased cellular uptake and metabolism in Allan-Herndon-Dudley syndrome (AHDS) due to a novel mutation in the MCT8 thyroid hormone transporter. *J Med Genet* 2006;**43**:457–60.
18. **Namba N,** Etani Y, Kitaoka T, Nakamoto Y, Nakacho M, Bessho K, Miyoshi Y, Mushiake S, Mohri I, Arai H, Taniike M, Ozono K. Clinical phenotype and endocrinological investigations in a patient with a mutation in the MCT8 thyroid hormone transporter. *Eur J Pediatr* 2008;**167**:785–91.
19. **Herzovich V,** Vaiani E, Marino R, Dratler G, Lazzati JM, Tilitzky S, Ramirez P, Iorcansky S, Rivarola MA, Belgorosky A. Unexpected peripheral markers of thyroid function in a patient with a novel mutation of the MCT8 thyroid hormone transporter gene. *Horm Res* 2007;**67**:1–6.

De novo mutations in epilepsy

Ohtahara syndrome and West syndrome are considered to be a continuum of early-onset epileptic encephalopathies, because the majority (75%) of Ohtahara syndrome cases evolve into West syndrome. Brain malformations are frequently associated with Ohtahara syndrome and West syndrome. The presence of cryptogenic cases suggests genetic factors may also be involved. However, most cases of these syndromes are sporadic, probably because of their poor clinical outcomes with severe psychomotor impairment.

De novo copy number variations (CNVs) and mutations are major causes of sporadic traits.[1] Their occurrence has been estimated to be 1.7×10^{-6} per locus and $2.2–4.0 \times 10^{-8}$ per nucleotide in a diploid embryo respectively, suggesting that an average newborn is expected to acquire approximately 0.86 amino acid altering mutations, and that de novo CNVs are more frequent than de novo mutations.[1–3] Increased availability of genomic microarrays, such as array comparative genomic hybridization, has facilitated the detection of de novo CNVs in which disease-causative genes may reside.

We have recently identified two disease-causative genes (*STXBP1* for Ohtahara syndrome and *SPTAN1* for a type of West syndrome) through identification of a de novo microdeletion at 9q33.3-q34.11 in one of four individuals (participant 1) with early-onset West syndrome with severe cerebral hypomyelination.[4–6] Among more than 40 genes within the deletion, we focused firstly on *STXBP1*, because it is involved in synaptic vesicle release and has brain-specific expression in both rodents and humans. Participant 1 was initially diagnosed with Ohtahara syndrome, which progressed to West syndrome at 3 months of age. *STXBP1* screening in other patients with Ohtahara syndrome with no brain anomalies led to the identification of four missense mutations, indicating that mutations in *STXBP1* cause cryptogenic Ohtahara syndrome.[4] To date, *STXBP1* abnormalities have been found in 19 out of 55 individuals (34.5%) with cryptogenic Ohtahara syndrome (including unpublished data).[7] Seventeen out of 19 deletions or mutations were confirmed as de novo events. The remaining two included an inherited mutation from the somatic-mosaic father, and an unconfirmed mutation due to unavailability of paternal DNA. Moreover, the clinical spectrum of *STXBP1* mutations has been shown to be broader. Aberrations of *STXBP1* were found in six out of 106 patients with early-onset epileptic encephalopathies (five mutations/deletions occured de novo).[8] Of note, the initial phenotype of five patients with *STXBP1* aberrations did not fit into either Ohtahara syndrome or West syndrome.[8] Furthermore, two de novo *STXBP1* mutations were also found in two out of 95 individuals with learning disability* and non-syndromic epilepsy.[9] These findings indicated that CNV and mutation screening in *STXBP1* should be considered in children with early-onset seizures.

Were there *STXBP1* mutations in the remaining three participants with early-onset West syndrome with severe cerebral hypomyelination? We could not find any *STXBP1* abnormalities in two of the remaining three participants (one was unavailable). While most patients with *STXBP1* mutations showed normal myelination, participant 1 additionally showed severe hypomyelination of the cerebral cortex and a thin corpus callosum at 12 months of age.[5] Therefore we hypothesized that another gene within the deletion may contribute to severe hypomyelination in participant 1. The *SPTAN1* gene encoding α-II spectrin appeared to be a primary candidate because zebrafish α-II spectrin mutants showed impaired myelination, and de novo in-frame mutations in *SPTAN1* were identified in the remaining two participants, suggesting that mutations in *SPTAN1* cause early-onset West syndrome with severe hypomyelination. Our identification of two disease genes from one de novo deletion in a single case may be a rare event; however, it should be emphasized that careful evaluation of clinical and molecular data in detail may reveal occult, yet important, findings.

In addition to *STXBP1* and *SPTAN1*, de novo mutations in *SCN1A*, *CDKL5*, and *ARX* genes have been reported in early-onset epileptic encephalopathies. Thus, it is likely that de novo mutations of known and unknown causative genes are a common cause of early-onset epileptic encephalopathies, which mostly occur sporadically. Recent progress in massively parallel DNA sequencing enables us to rapidly detect point mutations, and de novo mutations could be systemically identified by family-based exome sequencing (using trios: one patient and parents).[10] Together with genomic microarray, exome sequencing is likely to be provided as a clinical service in the near future, and will undoubtedly demonstrate important roles of de novo CNVs and mutations in early-onset epileptic encephalopathies.

HIROTOMO SAITSU
NAOMICHI MATSUMOTO
Department of Human Genetics, Graduate School of Medicine, Yokohama City University, Yokohama, Japan.

doi: 10.1111/j.1469-8749.2011.03994.x

*North American usage: mental retardation.

© The Authors. Developmental Medicine & Child Neurology © 2011 Mac Keith Press

REFERENCES

1. Lupski JR. Genomic rearrangements and sporadic disease. *Nat Genet* 2007; **39:** S43–7.
2. Lynch M. Rate, molecular spectrum, and consequences of human mutation. *Proc Natl Acad Sci USA* 2010; **107:** 961–8.
3. Roach JC, Glusman G, Smit AF, et al. Analysis of genetic inheritance in a family quartet by whole-genome sequencing. *Science* 2010; **328:** 636–9.
4. Saitsu H, Kato M, Mizuguchi T, et al. De novo mutations in the gene encoding STXBP1 (MUNC18-1) cause early infantile epileptic encephalopathy. *Nat Genet* 2008; **40:** 782–8.
5. Tohyama J, Akasaka N, Osaka H, et al. Early onset West syndrome with cerebral hypomyelination and reduced cerebral white matter. *Brain Dev* 2008; **30:** 349–55.
6. Saitsu H, Tohyama J, Kumada T, et al. Dominant-negative mutations in alpha-II spectrin cause West syndrome with severe cerebral hypomyelination, spastic quadriplegia, and developmental delay. *Am J Hum Genet* 2010; **86:** 881–91.
7. Saitsu H, Kato M, Okada I, et al. *STXBP1* mutations in early infantile epileptic encephalopathy with suppression-burst pattern. *Epilepsia* 2010; **51:** 2397–405.
8. Deprez L, Weckhuysen S, Holmgren P, et al. Clinical spectrum of early-onset epileptic encephalopathies associated with STXBP1 mutations. *Neurology* 2010; **75:** 1159–65.
9. Hamdan FF, Piton A, Gauthier J, et al. De novo STXBP1 mutations in mental retardation and nonsyndromic epilepsy. *Ann Neurol* 2009; **65:** 748–53.
10. Vissers LE, de Ligt J, Gilissen C, et al. A de novo paradigm for mental retardation. *Nat Genet* 2010; **42:** 1109–12.

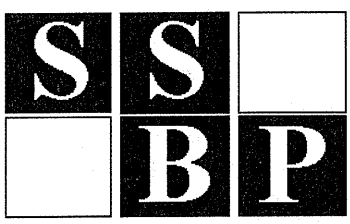

SOCIETY FOR THE STUDY OF BEHAVIOURAL PHENOTYPES

An International Organisation

The SSBP is a Registered Charity: Charity No: 1013849

14th International SSBP Research Symposium

Translating Genetics to Phenotype: Implications for Management

Research Symposium 5–6 October, Educational Day 7 October 2011
Brisbane, Australia

Earlybird registration deadline: 31 August 2011

http://www.ssbpconference.org/

CLINICAL GENETICS An International Journal of Genetics, Molecular and Personalized Medicine

Clin Genet 2011: 80: 161–166
Printed in Singapore. All rights reserved

© 2011 John Wiley & Sons A/S

CLINICAL GENETICS
doi: 10.1111/j.1399-0004.2011.01721.x

Short Report

Exome sequencing of two patients in a family with atypical X-linked leukodystrophy

Tsurusaki Y, Okamoto N, Suzuki Y, Doi H, Saitsu H, Miyake N, Matsumoto N. Exome sequencing of two patients in a family with atypical X-linked leukodystrophy.
Clin Genet 2011: 80: 161–166. © John Wiley & Sons A/S, 2011

We encountered a family with two boys similarly showing brain atrophy with reduced white matter, hypoplasia of the brain stem and corpus callosum, spastic paralysis, and severe growth and mental retardation without speaking a word. The phenotype of these patients was not compatible with any known type of syndromic leukodystrophy. Presuming an X-linked disorder, we performed next-generation sequencing (NGS) of the transcripts of the entire X chromosome. A single lane of exome NGS in each patient was sufficient. Six potential mutations were found in both affected boys. Two missense mutations, including c.92T>C (p.V31A) in *L1CAM*, were potentially pathogenic, but this remained inconclusive. The other four could be excluded. Because the patients did not show adducted thumbs or hydrocephalus, the *L1CAM* change in this family can be interpreted as different scenarios. Personal genome analysis using NGS is certainly powerful, but interpretation of the data can be a substantial challenge requiring a lot of tasks.

Conflict of interest

None of the authors have any conflicts of interest to disclose.

Y Tsurusaki[a], N Okamoto[b], Y Suzuki[c], H Doi[a], H Saitsu[a], N Miyake[a] and N Matsumoto[a]

[a]Department of Human Genetics, Yokohama City University Graduate School of Medicine, Kanazawa-ku, Yokohama, Japan, and [b]Department of Medical Genetics, and [c]Department of Pediatric Neurology, Osaka Medical Center and Research Institute for Maternal and Child Health, Murodo-cho, Izumi, Japan

Key words: atypical phenotype – exome sequencing – *L1CAM* – X-linked leukodystrophy

Corresponding author: Naomichi Matsumoto, Department of Human Genetics, Yokohama City University Graduate School of Medicine, 3-9 Fukuura, Kanazawa-ku, Yokohama 236-0004, Japan.
Tel.: +81-45-787-2606;
fax: +81-45-786-5219;
e-mail: naomat@yokohama-cu.ac.jp

Received 4 May 2011, revised and accepted for publication 31 May 2011

Focused/selected gene and genomic characterization has usually been carried out in clinically homogeneous groups of multiple affected samples to make identification of genetic abnormalities more efficient. Microarrays and next-generation sequencing (NGS) have provided new avenues for human genetic research (1–6). Using such new technologies, researchers are able to analyze small numbers of patients on a genome-wide scale. Even very rare cases (such as when only a few compatible patients are available or atypical patients showing no similar phenotypes) can be realistic targets of genetic research, as the new technologies can identify aberrations in a single gene from within virtually the whole genome; this could not be achieved with conventional techniques.

We encountered a family with two affected males showing atypical leukodystrophy. The phenotype of these patients did not match any known type of syndromic leukodystrophy. Because we presumed that abnormality of an X-linked gene caused the atypical leukodystrophy in this family, we performed exome sequencing of most of the X-chromosome transcripts and identified an unexpected gene mutation in these patients.

Materials and methods

A family with atypical X-linked leukodystrophy

Two brothers, II-1 currently aged 19 years and II-2 currently aged 17 years, who have unrelated healthy parents, presented with similar clinical

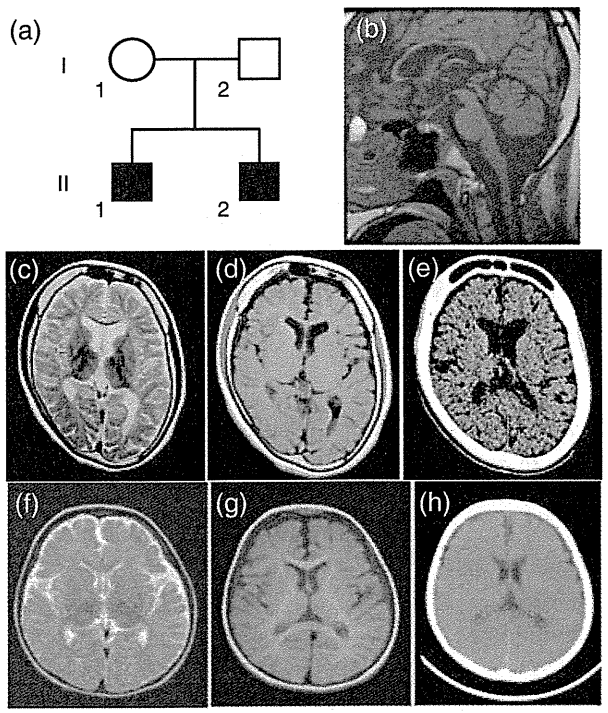

Fig. 1. Clinical features of the family. Familial pedigree (**a**). Brain magnetic resonance imaging (MRI) (**b**: T1-weighted image, **c**: T2-weighted image, **d**: T1-weighted image) of individual II-1 at 16 years old showing hypoplasia of the white matter, the brain stem and the corpus callosum. Brain computed tomographic (CT) images of individual II-1 at 19 years old (**e**) indicating a thick calvarium with enlarged frontal sinus as well as calcification of the choroid plexus in the atrophic brain. Brain MRI (**f**: T2-weighted image, **g**: T1-weighted image) of individual II-2 at 2 years old, also displaying hypoplasia of the white matter. Brain CT image of individual II-2 at 5 years old (**h**), also showing a thick calvarium.

features. Their mother did not show any neurological abnormalities (Fig. 1a).

Patient II-1

Patient II-1's birth weight was 2840 g at 40 weeks of gestational age. He had congenital nystagmus. He sat unsupported at 7 months old but after this his developmental milestones were delayed. He could creep at 18 months old. Spastic paralysis, especially in the lower extremities, became apparent. He was unable to stand unsupported. His mental development was severely delayed, and he needed special education from elementary school. He had suffered generalized epileptic seizures since he was 10 years old. He was confined to a wheelchair. He had severe mental retardation without speaking a word. His developmental quotient (DQ) at 9 years old was 19 by the Japanese standard method. Severe growth retardation [143 cm (<3%), 24 kg (<3%), occipitofrontal head circumference 49 cm (<3%) at 19 years] was also noted. He did not have dysmorphic features. Blood analysis revealed microcytic anemia [hemoglobin (Hb) 13.4 g/dl, mean corpuscular volume (MCV) (of red blood cell) 70.4 fl (normal: 89–99 fl), mean corpuscular hemoglobin (MCH) (of red blood cell) 23.1 pg (normal: 29–35 pg)] without any evidence of hemolysis or iron deficiency. Hormonal examination indicated that the levels of luteinizing hormone, follicle-stimulating hormone, and thyroid-stimulating hormone were all low [0.9 mIU/ml (normal: 1.2–8.0 mIU/ml), 2.5 mIU/ml (normal: 2.3–15.1 mIU/ml), <0.01 μIU/ml (normal: 0.5–5.0 μIU/ml), respectively]. He showed delayed puberty with small testes. Pubic hair only appeared at 17 years old. His bone age at 18 years old was 12.6 years (67%). Brain magnetic resonance imaging (MRI) at 16 years old revealed brain atrophy associated with reduced white matter and hypoplasia of the brain stem and the corpus callosum (Fig. 1b–d). No hydrocephalus or adducted thumb was observed. Brain computed tomography (CT) at 19 years old showed a thick calvarium with enlarged frontal sinus as well as calcification of the cerebellar tentorium and the choroid plexus (Fig. 1e).

Patient II-2

Patient II-2's birth weight was 2910 g at 37 weeks of gestational age. Developmental delay was apparent since he was 10 months old. Spastic paralysis (especially in the lower extremities), confinement to a wheelchair, severe mental retardation without speaking a word (DQ = 5 at 17 years old), and severe growth retardation [130 cm (<3%) and 27 kg (<3%) at 17 years] were phenotypes shared with his brother (II-1). Blood analysis revealed microcytic anemia (Hb 12.0 g/dl, MCV 61.1 fl, MCH 19.0 pg) without any evidence of hemolysis or iron deficiency. Hormonal examination indicated that the levels of luteinizing hormone, follicle-stimulating hormone, and thyroid-stimulating hormone were relatively low (1.9 mIU/ml, 4.2 mIU/ml, <0.23 μIU/ml, respectively). He also showed delayed puberty with small testes. Pubic hair appeared only at 17 years old. His bone age at 17 years old was 11 years (65%). Brain MRI at 2 years old revealed brain atrophy associated with reduced white matter and hypoplasia of the brain stem and corpus callosum (Fig. 1f,g). Brain CT at 5 years old showed a thick calvarium (Fig. 1h). No hydrocephalus or adducted thumb was observed. Most of the clinical features were similar to those of his brother except for the absence of nystagmus in patient II-2.

Genome-wide SNP genotyping

Genome-wide single-nucleotide polymorphism (SNP) genotyping was performed on individuals I-2, II-1, and II-2 using a GeneChip™ Human Mapping 10K Array Xba 142 2.0 (Affymetrix, Inc., Santa Clara, CA), according to the manufacturer's protocols. Mendelian error in the pedigree to exclude conflicted SNPs was checked using GCOS 1.2 (GeneChip Operating Software; Affymetrix) and batch analysis in GTYPE 4.0 (GeneChip Genotyping Analysis Software; Affymetrix), with the default setting for the mapping algorithm. The linked region, with SNP genotypes shared between individuals II-1 and II-2, was checked manually.

Genomic partitioning, short-read sequencing, and sequence alignment

Three micrograms of genomic DNA from the affected brothers (II-1 and II-2) was processed using a SureSelect X Chromosome test kit (1582 transcripts covering 3053 kb) (Agilent Technologies, Santa Clara, CA), according to the manufacturer's instructions. Captured DNAs were analyzed using an Illumina GAIIx (Illumina, Inc., San Diego, CA). We used only one of the eight lanes in the flow cell (Illumina) for paired-end, 76-bp reads per sample. Image analysis and base-calling were performed using sequence control software (SCS) real-time analysis and off-line BASECALLER software v1.8.0 (Illumina). Reads were aligned to the human reference genome (UCSC hg19, NCBI build 37.1) using the ELANDv2 algorithm in CASAVA_v1.7.0 (Illumina). The ELANDv2 algorithm can align 100-bp reads to a reference sequence and split the reads into multiple seeds.

Mapping strategy and variant annotation

Approximately 57.5 million reads from individual II-1 and 71.1 million reads from individual II-2 that passed the quality control (Path Filter) were mapped to the human reference genome using mapping and assembly with quality (MAQ) (7) (Fig. 2). MAQ was able to align 51 720 952 and 65 990 660 reads to the whole genome for individuals II-1 and II-2, respectively; these were then statistically analyzed for coverage using a script created by BITS Co., Ltd. (Tokyo, Japan). SNPs and insertions/deletions were extracted from the alignment data using an original script created by BITS Co., Ltd., along with information on the registered SNPs (dbSNP 131). A consensus quality score of 40 or more was used for the SNP analysis in MAQ. SNPs in MAQ-passed reads were annotated using the SeattleSeq website (http://gvs.gs.washington.edu/SeattleSeqAnnotation/). Variants found by each informatics method were selected in terms of location on chromosome X, unregistered variants (excluding registered SNPs), variants in known genes, variants in coding regions, variants excluding synonymous changes, and variants with an allele frequency of at least 90% (assuming a homozygous mutation). NEXTGENE software v2.0 (SoftGenetics, State College, PA) was also used to analyze the reads, with a default setting. Variants found by both of the informatics methods were selected. The variants found in common between individuals II-1 and II-2 were focused on, and confirmed as true positives by Sanger sequencing of polymerase chain reaction (PCR) products amplified from patient genomic DNA, except for variants within genes at segmental duplications. The pathological significance of the variants was evaluated using four different websites: POLYPHEN (Polymorphism Phenotyping; http://genetics.bwh.harvard.edu/pph/index.html), POLYPHEN-2 (http://genetics.bwh.harvard.edu/pph2/index.shtml), SIFT (http://sift.jcvi.org/) (output values less than 0.05 are deleterious), and MUTATIONTASTER (http://neurocore.charite.de/MutationTaster/).

Capillary sequencing

Possible pathological variants were confirmed by Sanger sequencing using an ABI 3500xl or ABI3100 autosequencer (Life Technologies, Carlsbad, CA), following the manufacturer's protocol. Sequencing data were analyzed using SEQUENCHER software (Gene Codes Corporation, Ann Arbor, MI).

Expression studies

The relative mRNA levels of *TMEM187* in cDNA of various fetal and adult human tissues (Human MTC™ Panel I and Human Fetal MTC™ Panel; Clontech, Mountain View, CA) were determined by quantitative real-time reverse transcription–polymerase chain reaction (RT-PCR) using TaqMan gene expression assays (Hs01920894_s1 for *TMEM187* and Hs00357333_g1 for β-actin as a control) (Life Technologies).

Results and discussion

Our coverage analysis indicated that for individuals II-1 and II-2, 79.2% and 78.8%, respectively, of the entire X-chromosome coding sequence (CDS) were completely covered, and 88.5% and 88.5%,

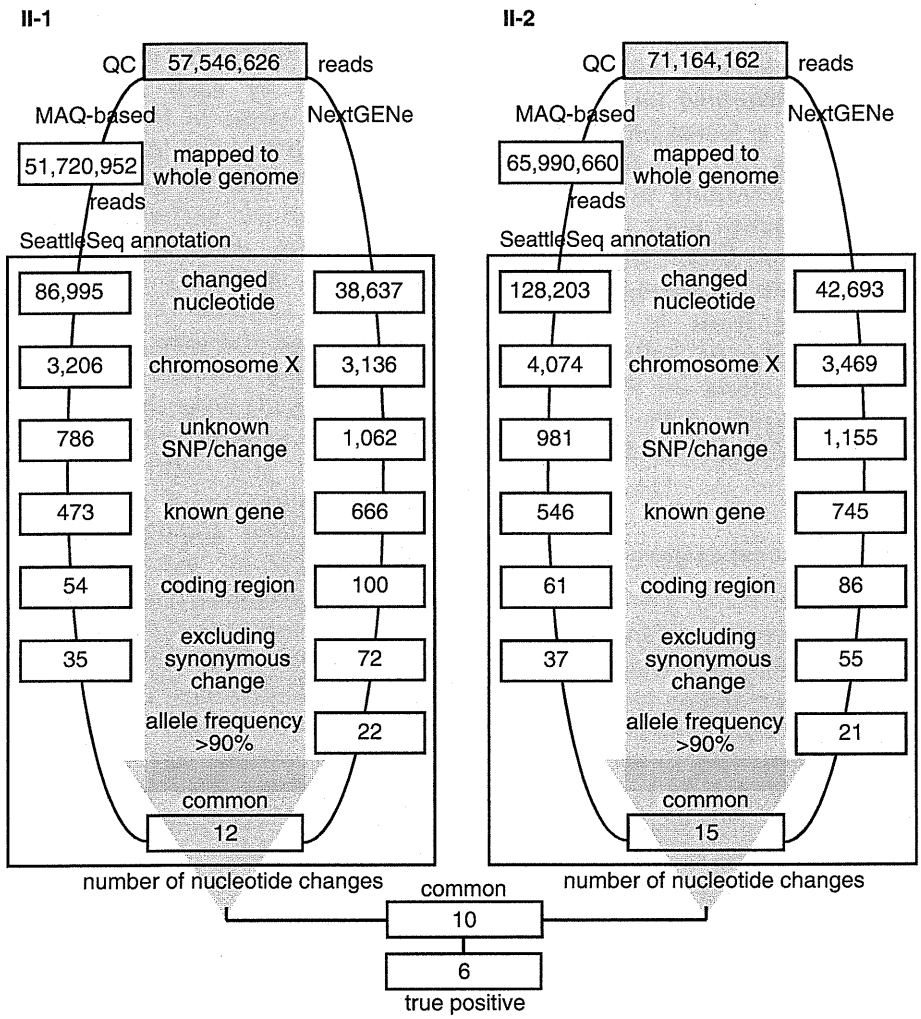

Fig. 2. Flow of informatics analysis. A MAQ-based method and NextGENe analysis were performed in individuals II-1 and II-2. The selection methods employed included variants compared with the human genome reference sequence, variants mapped to chromosome X, unknown variants [excluding registered single-nucleotide polymorphisms (SNPs)], variants in known genes, variants in coding regions, variants excluding synonymous changes, and variants common to the two informatics methods. Finally, the nucleotide changes in common between individuals II-1 and II-2 were focused on as potentially pathogenic mutations. True positive changes were confirmed by capillary sequencing of polymerase chain reaction (PCR) products amplified from genomic DNA.

respectively, of the CDS were at least 90% covered by reads. Using a single lane of sequencing per sample, the coverage with 20 reads or more comprised 89.6% and 89.7% of the CDS, and that with 100 reads or more comprised 87.6% and 89.7% of the CDS in individuals II-1 and II-2, respectively. SNP genotyping indicated that the region from rs727240 to rs721003 (UCSC genome browser hg19 assembly, chromosome X coordinates: 22131639–54454152; 32.2 Mb) was unlinked to the phenotype. Exome sequencing using two informatics methods successfully identified six potentially interesting changes as true positives in the linked region: *FAM123B* (RefSeq Gene ID NM_152424): c.85G>A (p.A29T), *FRMD7* (NM_194277): c.875T>C (p.L292P), *L1CAM* (NM_000425): c.92T>C (p.V31A), *TMEM187* (NM_003492): c.334G>A (p.A112T), *FLNA* (NM_001110556): c.1582G>A (p.V528M), and *LAGE3* (NM_006014): c.395G>A (p.R132Q).

The c.92T>C (p.V31A) variant in *L1CAM* was previously found in a patient with Hirschsprung disease, acrocallosal syndrome, and congenital hydrocephalus (8). *L1CAM* mutations cause a wide variety of clinical phenotypes: hydrocephalus due to stenosis of the aqueduct of Sylvius (MIM #307000), MASA syndrome (mental retardation, aphasia, shuffling gait, adducted thumb; MIM #303350), and X-linked agenesis of the corpus callosum (MIM #217990). Phenotypic variability, even within a family, has been noted, raising the caution that definite clinical diagnosis in single

Table 1. Characterization of nucleotide changes found by exome sequencing

	FAM123B	*FRMD7*	*L1CAM*	*TMEM187*	*FLNA*	*LAGE3*
Change	c.85G>A (p.A29T)	c.875T>C (p.L292P)	c.92T>C (p.V31A)	c.334G>A (p.A112T)	c.1582G>A (p.V528M)	c.395G>A (p.R132Q)
PolyPhen	Benign	Probably damaging	Benign	Benign	Possibly damaging	Benign
PolyPhen-2	Probably damaging	Probably damaging	Benign	Possibly damaging	Possibly damaging	Possibly damaging
SIFT	0.04	0.02	0.22	0.02	0.04	0.46
MutationTaster	Polymorphism	Disease causing	Disease causing	Polymorphism	Polymorphism	Polymorphism
Normal female	8/502[a]	2/502	2/502	1/502	15/502[a]	4/502
Normal male	1/118	0/117	0/118	0/118		1/86
Note		No nystagmus in II-2				

[a]Including one homozygous female. Underlining means that this result excludes the variant as potentially causative. Grayed shading indicates the variants that could not be excluded; between these two, the *L1CAM* variant is more likely to be causative.

cases is often impossible (9). Phenotypic features compatible with the *L1CAM* mutation in our patients include spastic paralysis, aphasia, severe mental and growth retardation, but atypical leukodystrophy and the absence of adducted thumbs were very rare or exceptional (9). A normal control study found that 2 of 251 normal females were heterozygous for this SNP, but none of 117 normal males carried the variant allele. One of the four web-based analyses of pathological significance (MutationTaster) indicated that this variant would be disease causing, while the others indicated that it would be benign (Table 1). X-linked hydrocephalus due to *L1CAM* mutations occurs in approximately 1/30 000 male births (10). Considering that the *L1CAM* mutation was found in 2/618 control alleles (0.32%), the change may be a rare polymorphism, a mutation causing lethality in the majority of affected males, or a mutation with low penetrance. Because we were unable to exclude this *L1CAM* change, its pathogenic status remains inconclusive.

We next examined c.85G>A in *FAM123B*, c.875T>C in *FRMD7*, c.1582G>A in *FLNA*, and c.395G>A in *LAGE3* in normal controls. The *FAM123B*, *FLNA*, and *LAGE3* variants were excluded as causative because a homozygous change was found in 1 of 251 female controls (*FAM123B* and *FLNA*) or a hemizygous change was found in 1 of 86 normal males (*LAGE3*). However, the thick calvarium in individuals II-1 and II-2 may be influenced by the *FAM123B* change, because it is causative for osteopathia striata with cranial sclerosis, an X-linked dominant disorder (MIM #300373) (11, 12). As the calvarium of the patients' mother having the heterozygous *FAM123B* change was not evaluated by CT, we could not confirm this possibility.

Only 2 of 251 control females carried the c.875T>C variant in *FRMD7* heterozygously, and none of 117 male controls carried this variant; thus, the pathogenicity of the *FMRD7* variant was inconclusive. Other *FRMD7* mutations cause X-linked congenital nystagmus 1 (MIM #310700) (13). However, the nystagmus found in individual II-1 was not observed in individual II-2, indicating that the variant in common between two brothers did not consistently cause nystagmus. Thus, it may not contribute to the phenotype in this family (Table 1).

We also evaluated the c.334G>A variant in *TMEM187*. Only 2 of 251 female controls carried this heterozygous change, and it was not found among 118 male controls. Two of the four programs (PolyPhen-2 and SIFT) indicated that it would be pathogenic. By Taqman assay, *TMEM187* was ubiquitously expressed in various fetal and adult tissues, including the brain (data not shown), leaving the effect of this mutation on the phenotype in these patients inconclusive (Table 1).

In conclusion, we found two possible but inconclusive variants in this family with two boys affected by atypical leukodystrophy. High-throughput technologies are clearly powerful to detect genomic changes, but evaluation of the data can be very difficult and should be performed cautiously. More knowledge of rare SNPs and mutations is absolutely necessary before any conclusions can be drawn.

Acknowledgements

We would like to thank the patients and their family members for their participation in this study. This work was supported by research grants from the Ministry of Health, Labour and Welfare

(to H. S., N. Miyake, and N. Matsumoto), the Japan Science and Technology Agency (to N. Matsumoto), a Grant-in-Aid for Scientific Research from the Japan Society for the Promotion of Science (to N. Matsumoto), and a Grant-in-Aid for Young Scientists from the Japan Society for the Promotion of Science (to H. D., N. Miyake, and H. S.).

References

1. Saitsu H, Kato M, Mizuguchi T et al. De novo mutations in the gene encoding STXBP1 (MUNC18-1) cause early infantile epileptic encephalopathy. Nat Genet 2008: 40: 782–788.
2. Check Hayden E. Genomics shifts focus to rare diseases. Nature 2009: 461: 458.
3. Biesecker LG. Exome sequencing makes medical genomics a reality. Nat Genet 2010: 42: 13–14.
4. Kuhlenbaumer G, Hullmann J, Appenzeller S. Novel genomic techniques open new avenues in the analysis of monogenic disorders. Hum Mutat 2011: 32: 144–151.
5. Miyake N, Kosho T, Mizumoto S et al. Loss-of-function mutations of CHST14 in a new type of Ehlers-Danlos syndrome. Hum Mutat 2010: 31: 966–974.
6. Ng SB, Bigham AW, Buckingham KJ et al. Exome sequencing identifies MLL2 mutations as a cause of Kabuki syndrome. Nat Genet 2010: 42: 790–793.
7. Li H, Ruan J, Durbin R. Mapping short DNA sequencing reads and calling variants using mapping quality scores. Genome Res 2008: 18: 1851–1858.
8. Nakakimura S, Sasaki F, Okada T et al. Hirschsprung's disease, acrocallosal syndrome, and congenital hydrocephalus: report of 2 patients and literature review. J Pediatr Surg 2008: 43: E13–E17.
9. Rietschel M, Friedl W, Uhlhaas S, Neugebauer M, Heimann D, Zerres K. MASA syndrome: clinical variability and linkage analysis. Am J Med Genet 1991: 41: 10–14.
10. Rosenthal A, Jouet M, Kenwrick S. Aberrant splicing of neural cell adhesion molecule L1 mRNA in a family with X-linked hydrocephalus. Nat Genet 1992: 2: 107–112.
11. Viot G, Lacombe D, David A et al. Osteopathia striata cranial sclerosis: non-random X-inactivation suggestive of X-linked dominant inheritance. Am J Med Genet 2002: 107: 1–4.
12. Jenkins ZA, van Kogelenberg M, Morgan T et al. Germline mutations in WTX cause a sclerosing skeletal dysplasia but do not predispose to tumorigenesis. Nat Genet 2009: 41: 95–100.
13. Tarpey P, Thomas S, Sarvananthan N et al. Mutations in FRMD7, a newly identified member of the FERM family, cause X-linked idiopathic congenital nystagmus. Nat Genet 2006: 38: 1242–1244.

REPORT

Exome Sequencing Reveals a Homozygous *SYT14* Mutation in Adult-Onset, Autosomal-Recessive Spinocerebellar Ataxia with Psychomotor Retardation

Hiroshi Doi,[1,2] Kunihiro Yoshida,[3] Takao Yasuda,[4] Mitsunori Fukuda,[4] Yoko Fukuda,[5] Hiroshi Morita,[6] Shu-ichi Ikeda,[6] Rumiko Kato,[7] Yoshinori Tsurusaki,[1] Noriko Miyake,[1] Hirotomo Saitsu,[1] Haruya Sakai,[1] Satoko Miyatake,[1] Masaaki Shiina,[8] Nobuyuki Nukina,[9] Shigeru Koyano,[2] Shoji Tsuji,[5] Yoshiyuki Kuroiwa,[2] and Naomichi Matsumoto[1,*]

Autosomal-recessive cerebellar ataxias (ARCAs) are clinically and genetically heterogeneous disorders associated with diverse neurological and nonneurological features that occur before the age of 20. Currently, mutations in more than 20 genes have been identified, but approximately half of the ARCA patients remain genetically unresolved. In this report, we describe a Japanese family in which two siblings have slow progression of a type of ARCA with psychomotor retardation. Using whole-exome sequencing combined with homozygosity mapping, we identified a homozygous missense mutation in *SYT14*, encoding synaptotagmin XIV (SYT14). Expression analysis of the mRNA of *SYT14* by a TaqMan assay confirmed that *SYT14* mRNA was highly expressed in human fetal and adult brain tissue as well as in the mouse brain (especially in the cerebellum). In an in vitro overexpression system, the mutant SYT14 showed intracellular localization different from that of the wild-type. An immunohistochemical analysis clearly showed that SYT14 is specifically localized to Purkinje cells of the cerebellum in humans and mice. Synaptotagmins are associated with exocytosis of secretory vesicles (including synaptic vesicles), indicating that the alteration of the membrane-trafficking machinery by the *SYT14* mutation may represent a distinct pathomechanism associated with human neurodegenerative disorders.

Hereditary ataxias are genetically heterogeneous neurological disorders: autosomal-dominant, autosomal-recessive, X-linked, and mitochondrial types are known. Among ataxias, spinocerebellar ataxia (SCA) is relatively common and involves the cerebellum, brainstem, or spinocerebellar long tracts.[1] Autosomal-recessive cerebellar ataxias (ARCAs) are generally associated with diverse neurological and nonneurological attributes, resulting in complex phenotypes. ARCAs include congenital nonprogressive ataxias and progressive ataxias such as SCAs.[2] The clinical onset of ARCAs usually occurs before the age of 20, even if congenital types are excluded.[1,3,4] Currently, more than 20 defective genes have been identified in ARCAs.[2,5,6] These genes have variable recognized functions, including those involving mitochondrial energy generation, cellular metabolisms, DNA repair, chaperone-mediated protein folding, RNA processing, and ion channels.[1,3,6] Approximately half of the patients with ARCAs remain genetically unresolved.[4] Therefore, more investigations of ARCAs are required. In this study, we describe a Japanese family with two siblings showing psychomotor retardation and the slowly progressive type of SCA without involvement of pyramidal tracts or peripheral nerves. Exome sequencing combined with homozygosity mapping successfully identified a causative mutation.

Clinical information and blood materials were obtained from the family members after written informed consent was secured. Experimental protocols were approved by IRBs of the Yokohama City University and the Shinshu University. Among the children of first-cousin parents, two siblings (IV-3 and IV-4) were found to be affected, whereas the other two (IV-1 and IV-2) were healthy (Figure 1A). No similar patients were recognized within the family. IV-3 had mild psychomotor retardation from childhood. He found a job after graduating from an ordinary junior high school. At 35 years of age, he lost his job for social reasons. Although he had some gait disturbances from childhood, he could independently go shopping and walk a dog even after leaving his occupation. At the age of ~56, he developed obvious gait unsteadiness and began to stumble frequently. At 58, he started to choke on food. These symptoms gradually worsened, and he sought medical examination at 59 years of age. He displayed disturbances of smooth-pursuit eye movements, dysarthria, mild limb ataxia, and moderate truncal ataxia. His muscle tone was normal, and no involuntary

[1]Department of Human Genetics, Graduate School of Medicine, Yokohama City University, 3-9 Fukuura, Kanazawa-ku, Yokohama 236-0004, Japan; [2]Department of Clinical Neurology and Stroke Medicine, Graduate School of Medicine, Yokohama City University, 3-9 Fukuura, Kanazawa-ku, Yokohama 236-0004, Japan; [3]Division of Neurogenetics, Department of Brain Disease Reseach, Shinshu University School of Medicine, 3-1-1 Asahi, Matsumoto, Nagano 390-8621, Japan; [4]Laboratory of Membrane Trafficking Mechanisms, Department of Developmental Biology and Neuroscience, Graduate School of Life Sciences, Tohoku University, Aobayama, Aoba-ku, Sendai, Miyagi 980-8578, Japan; [5]Department of Neurology, Graduate School of Medicine, The University of Tokyo, 7-3-1 Hongo, Bunkyo-ku, Tokyo 113-8655, Japan; [6]Department of Medicine (Neurology & Rheumatology), Shinshu University School of Medicine, 3-1-1 Asahi, Matsumoto, Nagano 390-8621, Japan; [7]Department of Pediatrics, National Higashi-Saitama Hospital, 4147 Kurohama, Hasuda 349-0196, Japan; [8]Department of Biochemistry, Graduate School of Medicine, Yokohama City University, 3-9 Fukuura, Kanazawa-ku, Yokohama 236-0004, Japan; [9]Laboratory for Structural Neuropathology, Brain Science Institute, RIKEN, 2-1 Hirosawa, Wako 351-0198, Japan
*Correspondence: naomat@yokohama-cu.ac.jp
DOI 10.1016/j.ajhg.2011.07.012. ©2011 by The American Society of Human Genetics. All rights reserved.

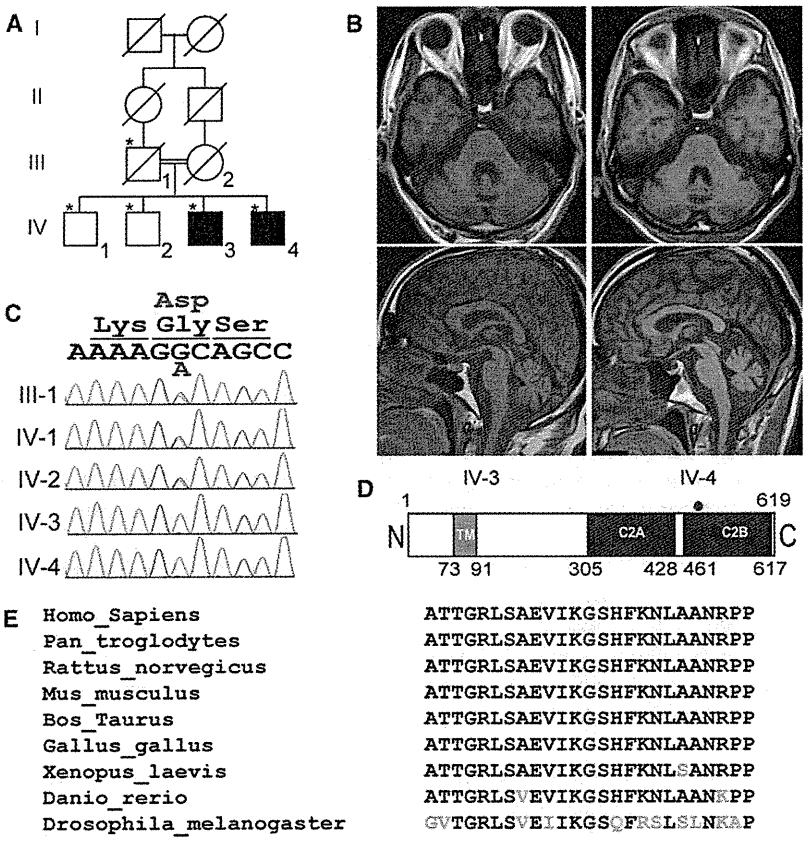

Figure 1. Familial Pedigree, Brain MRI of Patients, and the *SYT14* Mutation Identified

(A) Familial pedigree of the patients with autosomal-recessive spinocerebellar ataxia. *An asterisk indicates members whose genomic DNA was available for this study.

(B) Brain MRI of IV-3 at 59 years of age (left panels) and IV-4 at 56 years of age (right panels). Axial (upper panels) and sagittal (lower panels) sections of a T1-weighted image are shown.

(C) Electropherograms of unaffected (III-1, IV-1, and IV-2) and affected (IV-3 and IV-4) members, who show the mutation.

(D) Schematic presentation of SYT14. The red dot indicates the location of the mutation in the C2B domain.

(E) The missense mutation occurred at an evolutionarily conserved amino acid (in red).

movements were observed. Laboratory examination, including analysis of serum albumin, vitamin E, and α-fetoprotein, was normal. A nerve-conduction study (NCS) indicated no neuropathy. No retinitis pigmentosa was recognized by ophthalmologic evaluation. Brain magnetic resonance imaging (MRI) revealed mild atrophy of the cerebellar vermis and hemispheres but no apparent atrophy of the brain stem or the cerebral cortex. (Figure 1B, left panels).

Similar to IV-3, IV-4 also had psychomotor retardation from childhood, but this retardation was more severe than that of IV-3. After graduation from a school for disabled children at the age of 15, he entered a facility for disabled people. He showed gait disorder, but he was able to walk without a cane. At an age of ~50, his gait disturbance worsened, and he went for a medical check at a hospital when he was 56 years old. He displayed disturbance of smooth-pursuit eye movements, gaze-evoked horizontal nystagmus, dysarthria, mild limb ataxia, and moderate truncal ataxia. No involuntary movements were observed. His laboratory tests, including those for serum albumin, vitamin E, and α-fetoprotein, were normal. NCS was normal. A brain MRI was similar to that of IV-3 (Figure 1B, right panels). The clinical manifestations of these two patients are summarized in Table 1.

To search for the disease locus, we conducted genome-wide SNP genotyping of III-1, IV-1, IV-2, IV-3, and IV-4 by using the Genome-wide Human SNP Array 6.0 (SNP 6.0 array) (Affymetrix, Inc., Santa Clara, CA) according to the manufacturer's instructions. Then, SNP 6.0 array data were subjected to homozygosity mapping with HomozygosityMapper software.[7] For the linkage analysis, a subset of 7339 SNPs with high heterozygosity (mean heterozygosity 0.49) was extracted from the SNP 6.0 array data with the program Linkdatagen, for which the bin size was set to 0.5cM and the allele frequency of the Japanese population was used.[8] The multipoint LOD score was calculated with Allegro version 2[9] on the basis of the model of autosomal-recessive and X-linked-recessive inheritance, respectively. In both models, complete penetrance and a disease-allele frequency of 0.0001 were adopted. The homozygosity mapping revealed a total of three regions, which together were approximately 11.35 Mb in size, as candidate loci, where genes known to be mutated in ARCA did not exist (Table 2). In the model of autosomal-recessive inheritance, a total of ten regions with a LOD score greater than 1.5 in the multipoint linkage analysis were identified (Table S1). The three homozygous regions in accordance with the linked regions still survived as candidate regions. On the basis of X-linked recessive inheritance, a total of three regions with positive LOD scores (maximum LOD score = 0.9031) were highlighted; together, these three regions were approximately 101.03 Mb (Table S1).

To find a gene mutation within the candidate loci, we performed whole-exome sequencing on IV-3 and IV-4. Three micrograms of genomic DNA was processed with the SureSelect Human All Exon Kit v.1 (approximately 180,000 exons covering 38 Mb of the CCDS database) (Agilent Technologies, Santa Clara, CA) according to the manufacturer's instructions. Captured DNAs were sequenced on an Illumina GAIIx (Illumina, San Diego, CA) with 76 bp pair-end reads. Of the possible eight lanes of the flow cell, two lanes for IV-3 and three lanes for IV-4 (Illumina) were used. Image analysis and base calling

Table 1. Clinical Features of the Patients

Clinical Features	IV-3	IV-4
Age at present	61	58
Sex	male	male
Age of obvious ataxia	56	around 50
Mental retardation	mild	moderate
Ocular apraxia	no	no
Ophthalmoplegia	no	no
Nystagmus	no	+
Dysarthria	+	+
Truncal ataxia	++	++
Limb ataxia	+	+
Extrapyramidal signs	no	no
Involuntary movements	no	no
Sensory involvements	no	no
Tendon reflex	normal-increased	normal-decreased
Plantar responses	normal	normal
Peripheral neuropathy	no	no
Pes cavus	no	no
SARA[a]	12/40	15/40
Cerebellar atrophy on MRI	+	+
others	normal level of serum albumin, vitamin E, and α-fetoprotein	normal level of serum albumin, vitamin E, and α-fetoprotein

[a] SARA: Scale for the assessment and rating of ataxia.[32]

Table 2. Regions of Homozygosity

Chromosome	Chromosomal Position (rsID)	Size (Mb)	LOD
1	207226930 (rs2761781)–213992561 (rs1857229)	6.77	2.0537
4	181929079 (rs918401)–185188999 (rs7690914)	3.26	2.0554
22	45676443 (rs3905396)–47003473 (rs2013591)	1.33	2.0545

Regions of homozygosity were identified by HomozygosityMapper, and the LOD scores were calculated by multipoint linkage analysis, for which SNPs were extracted from SNP 6.0 array data via Linkdatagen.

were performed by sequence control software (SCS) real-time analysis (Illumina) and CASAVA software v1.6 (Illumina). Reads were aligned to the human reference genome sequence (UCSC hg18, NCBI build 36.1) via the ELAND v2 program (Illumina). Coverage was calculated statistically with a script created by BITS (Tokyo, Japan). Approximately 71 million reads from IV-3 and 148 million reads from IV-4 (these numbers of reads passed quality-control [Path Filter]) were mapped to the human reference genome with Mapping and Assembly with Qualities (MAQ)[10] and NextGENe software v2.00 (SoftGenetics, State College, PA) under the default settings. MAQ aligned 59,491,138 and 126,159,746 reads to the whole genome for IV-3 and IV-4, respectively. A script created by BITS was used for extraction of SNPs and indels from the alignment data; dbSNP build 130 served as a reference for registered SNPs. A consensus quality score of 40 or more was adopted for the SNP analysis in MAQ. Coverage analysis revealed that 65.0% (IV-3) and 71.3% (IV-4) of the coding sequences (CDS) were completely covered (100%), and 77.7% (IV-3) and 80.3% (IV-4) of CDS were mostly covered by reads (90% or more) through the whole genome. 79.0% (IV-3) and 79.7% (IV-4) of total CDS were covered by ten reads or more (50 reads or more in 66.4% and 77.1%, respectively).

To identify the pathogenic mutation, we adopted a prioritization scheme, which has been used in recent studies.[11–13] First, we excluded the variants registered in dbSNP130 from all the detected variants and then picked up homozygous mutations and variants in coding regions and the intronic regions within 50 bp from coding sequences. Of the homozygous mutations and variants, we focused on those within the candidate regions. As a result, only two missense mutations or variants, p.Gly484Asp (c.1451G>A) (NM_001146261.1) in exon 8 of *SYT14* (1q32.2, [MIM 610949]) and p.Gln4203Arg (c.12608A>G) (NM_206933.2) in exon 63 of *USH2A* (1q41, [MIM 608400]) remained as candidates for both cases (Table S2). Sanger sequencing with ABI 3500xL (Life Technologies, Carlsbad, CA) confirmed that the c.1451G>A of *SYT14* was homozygous in IV-3 and IV-4 and heterozygous in III-1 (father), IV-1, and IV-2, whereas the c.12608A>G of *USH2A* was homozygous in IV-2 as well as IV-3 and IV-4 (Figure 1C and data not shown). The *SYT14* missense mutation occurred at an evolutionarily conserved amino acid among different species and resides in the second C2 (C2B) domain (Figures 1D and 1E). In silico analysis incorporating different tools, including Polyphen, Polyphen2, SIFT, and Align GVGD, consistently indicated that the change was damaging (Table S3). The mutation was not detected in 576 Japanese control chromosomes, indicating that the mutation is very rare. On the basis of the X-linked recessive model, no pathological hemizygous mutation of protein-coding genes was detected in the possible candidate loci (Table S4).

We considered the *SYT14* mutation to be the causative agent and used the Sanger method to conduct mutation screening of all the coding regions of *SYT14* in 65 simplex SCA cases and 37 SCA familial cases, including three with autosomal-recessive inheritance. Only p.Gly183Glu (c.548G>A) was found in one family with autosomal-dominant SCA; however, the change was not consistent with the SCA phenotype in the family (Table S3). Thus, we could not detect any other pathological changes in *SYT14*. This was probably due to the small number of cases tested.

Synaptotagmin XIV (SYT14), which is encoded by *SYT14*, is a member of the synaptotagmins (SYTs), which are membrane-trafficking proteins, and SYT14 is conserved across many organisms.[14] Although the original report indicated that *SYT14* was not expressed in mouse brain,[14] multiple lines of evidence, including from the Allen brain Atlas, suggest that *SYT14* is expressed in the central nervous system (CNS) of the fly, mouse, and human brains.[15,16] To confirm *SYT14* expression in the CNS, we performed TaqMan quantitative real-time PCR analysis with cDNAs of adult human tissue (Human MTC Panel I, #636742) (Clontech Laboratories, Mountain View, CA), fetal human tissue (Human Fetal MTC Panel, #636747) (Clontech Laboratories), mouse tissue (Mouse MTC Panel I, #636745) (Clontech Laboratories), and various regions of the mouse brain (GSMBRSET) (NIPPON Genetics, Tokyo, Japan) as templates. Predesigned TaqMan probe sets for human *SYT14* (Hs00950169_m1), mouse *Syt14* (Mm00805319_m1), human *β-actin* (*ACTB*, 4326315E), and mouse *Actb* (43522341E) from Applied Biosystems were used. PCR reactions (total volume of 20 μl) contained 10 μl of the TaqMan Gene Expression Master Mix (Applied Biosystems), 1 μl of 20 × TaqMan reagents for *ACTB/Actb* and *SYT14/Syt14*, and 1 μl of cDNA (containing 1 ng cDNA in MTC panels and 25 ng cDNA in GSMBRSET) as the template. PCR was performed on a Rotor-Gene Q (QIAGEN, Valencia, CA) as follows: 2 min at 50°C and 10 min at 95°C, then 40 cycles of 95°C for 15 s and 60°C for 1 min. Expression levels were calculated with the Rotor-Gene Q Series Software (QIAGEN) by the $2^{-\Delta\Delta Ct}$ method. The cycling threshold (Ct) of the target gene was compared with the Ct of *ACTB* cDNA, and ΔCt was expressed as Ct of *SYT14* − Ct of *ACTB*. ΔΔCt was expressed as ΔCt of the control sample − ΔCt of each sample, and relative concentration was determined as $2^{-\Delta\Delta Ct}$. Expression in the kidney and the cerebral cortex was used as the control in Figures 2A–2D. *SYT14* was predominantly expressed in human adult and fetal brain tissues (Figures 2A and 2B). Even in mice, substantial expression in the brain was confirmed (but, not predominant) (Figure 2C). Among various brain regions in mice, *SYT14* was mostly expressed in the cerebellum (Figure 2D).

Intracellular distribution of SYT14 in cultured cells was investigated. The full-length *SYT14* PCR product amplified from human brain cDNA (MHS4426-99239810, Open Biosystems, Huntsville, AL) was used as a template and subcloned into pDONR221 (the entry vector of Gateway system, Invitrogen). We used site-directed mutagenesis to produce the *SYT14* mutant and variants by using a mutagenesis kit (Toyobo, Osaka, Japan). Variants include c.611C>T and c.810_812del, which are registered in dbSNP130, and c.548G>A, which was detected in an SCA patient with autosomal-dominant inheritance but did not segregate with the phenotype, indicating that it is nonpathogenic (Table S3). All constructs were verified by DNA sequencing. Each construct was recloned into the pEF-DEST51 mammalian expression vector (Invitrogen) and transfected to COS-1 cells with the FuGENE^{R}6 transfection reagent (Roche Applied Science, Mannheim, Germany) according to the manufacturer's instructions. Localization of the mutant (p.Gly484Asp) was clearly different from that of the wild-type and other (normal) variants. Whereas the wild-type and other variants were localized to the perinuclear and submembranous regions, p.Gly484Asp was localized in the cytoplasm (significant amounts were in the perinuclear region) but formed a characteristic reticular pattern without showing any submembranous distribution (Figures 2E and S2B). Confocal microscopic analysis showed that the p.Gly484Asp mutant was colocalized with an endoplasmic reticulum (ER) marker, protein disulfide isomerase (PDI), throughout the cells, whereas the wild-type colocalized with PDI dominantly in perinuclear regions (Figure 2F). immunoblot analysis combined with subcellular fractionation of the transfected cells further confirmed that the mutant was distributed differently from the wild-type. The wild-type and the mutant (p.Gly484Asp) were distributed in the nucleus and Golgi apparatus fractions; however, only the mutant was detected in microsome fractions containing ER fragments together with an ER membrane marker, calnexin (Figure S1).[17] These data suggest that improper folding of the mutant protein results in abnormal retention in the ER.

To investigate the effect of the p.Gly484Asp mutation in the C2B domain on phospholipid binding activity, we amplified cDNA of C2B domains from the wild-type and the p.Gly484Asp mutant from SYT14-expressing vectors by using the following primers: sense, 5′-GGATCCGAAA GTACATCCTCATGTCA-3′; and antisense, 5′-TCATGAC TCTAGCAACGCAT-3′. We then recloned the cDNA into *Escherichia coli* (*E. coli*) expressing vector (pGEX-4T-3). The C2B domain of SYT14 fused to glutathione S-transferase (GST) was expressed in *E. coli* JM109 and purified by standard protocols. Both GST-SYT14-C2B (WT) and GST-SYT14-C2B (p.Gly484Asp) could be mostly purified of contamination by degradation products, but the amount of GST-SYT14-C2B (p.Gly484Asp) obtained was at least four times smaller than that of GST-SYT14-C2B (WT) (data not shown). Liposome (phosphatidylcholine and phosphatidylserine, 1:1, w/w) cosedimentation assay with purified GST-SYT14-C2B was performed as described previously.[18] The result showed that the SYT14-C2B (p.Gly484Asp) bound liposomes similarly to SYT14-C2B (WT) (Figure 2G), indicating that the p.Gly484Asp mutation had no effect on the Ca^{2+}-independent phospholipid-binding activity of the SYT14-C2B domain.

The Allen Mouse Brain Atlas indicates that *Syt14* is expressed in Purkinje cells of the cerebellum in mice; however, SYT14 localization has not been fully investigated.[15] A rabbit polyclonal anti-SYT14 antibody (Ab-SYT14) was generated for immunoblotting and immunocytochemistry (Operon Biotechnologies, Tokyo, Japan) (Figure S2). Immunohistochemical analysis of mouse and human brains was

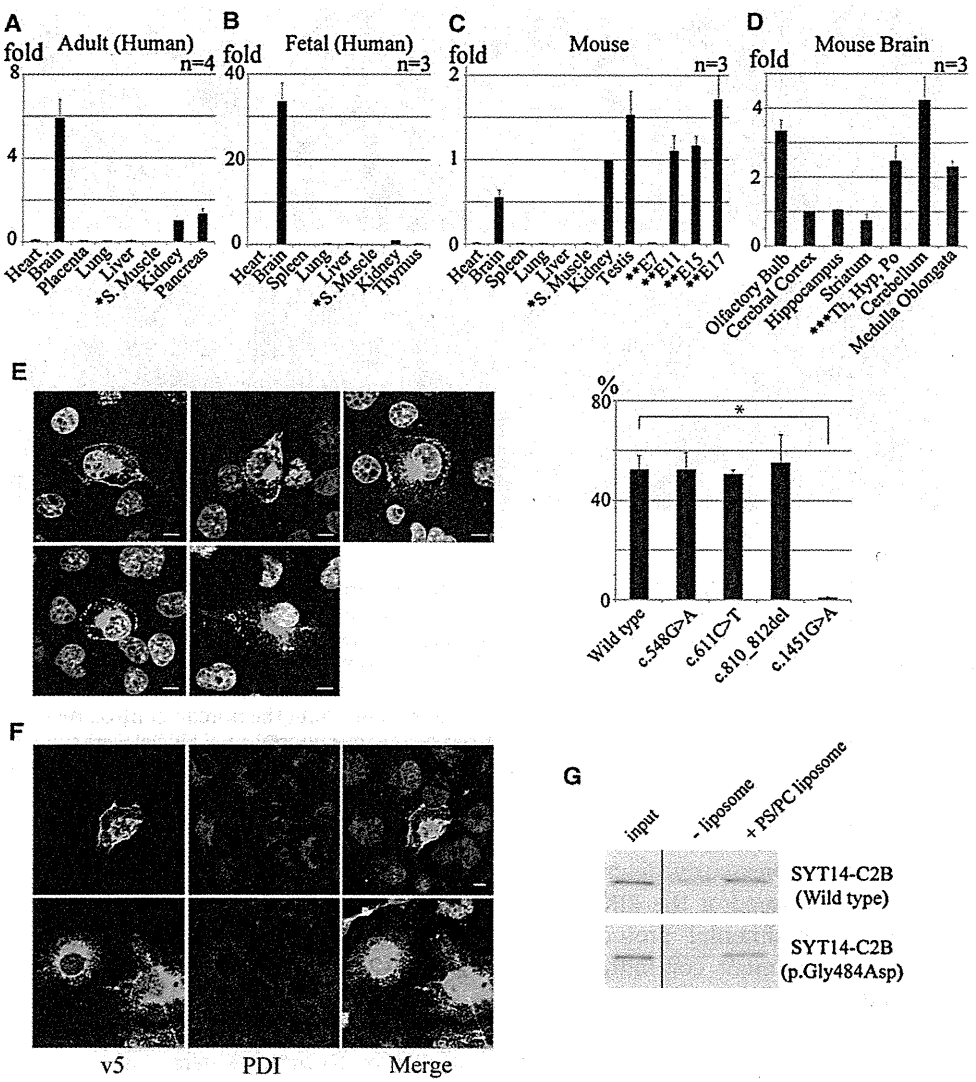

Figure 2. Expression Studies of *SYT14/Syt14* cDNA in Human and Mouse Tissues and Localization of SYT14 in Transfected COS-1 Cells
(A–D) The results of a TaqMan quantitative real-time PCR assay in which the first-strand cDNA of human adult tissues (A), human fetal tissues (B), mouse tissues (C), and various regions of mouse brain (D) were used as templates. The relative cDNA concentrations were determined from cDNA concentrations of the kidney (human adult tissues, human fetal tissues, and mouse tissues) or cerebral cortex (various regions of the mouse brain). Error bars represent the standard deviation. *S. Muscle indicates skeletal muscle. **E7, **E11, **E15, and **E17 indicate mouse embryos at 7, 11, 15, and 17 days of embryonic development, respectively. ***Th, Hyp and Po indicate thalamus, hypothalamus, and pons.
(E) Immunocytochemistry of COS-1 cells transfected with expression vectors of v5/His-tagged wild-type (upper left), p.Gly183Glu (c.548G>A) (upper middle), p.Pro203Leu (c.611C>T) (upper right), p.Glu270del (c.810_812del) (lower left), or p.Gly484Asp (c.1451G>A) (lower middle) SYT14. The SYT14 was detected with the anti-v5 antibody (Alexa fluor 488 as the secondary antibody). Nuclei were stained (white) with 4′,6-diamidino-2-phenylindole (DAPI). The horizontal bars indicate 10 μm. The bar graph indicates the ratio of the cells in which overexpressed proteins were accumulated in submembranous regions. A total of 120 cells per each transfectant in triplicated experiments were counted. Submembranous localization of the mutant (p.Gly484Asp) was mostly unseen, in contrast to the wild-type (*$p < 0.001$).
(F) Immunocytochemical analysis of COS-1 cells transfected with expression vectors of v5/His-tagged wild-type (upper panels) or the p.Gly484Asp mutant (lower panels). The SYT14 was detected with the anti-v5 antibody (Alexa fluor 488 as the secondary antibody), and PDI (protein disulfide isomerase) was visualized with an anti-PDI antibody (Alexa fluor 546 as the secondary antibody). Nuclei were stained (white) with DAPI. The scale bar represents 10 μm. The anti-v5 and anti-PDI antibodies and the Alexa-488-conjugated secondary antibody were all used at a dilution of 1:1000.
(G) Phospholipid binding activity of the C2B domain of the wild-type SYT14 and the p.Gly484Asp mutant. Liposomes and GST-fusion proteins (2 μg) were incubated in 50 mM HEPES-KOH (pH 7.2) in the presence of 2 mM EGTA for 15 min at room temperature. After centrifugation at 12,000 × *g* for 10 min, the supernatants (non-binding fraction) and pellets (phospholipid-binding fraction) were separated as described previously.[18] The pelleted samples and input samples (100 ng) were subjected to 10% SDS-PAGE followed by immunoblotting with horseradish peroxidase-conjugated anti-GST antibody (Santa Cruz Biotechnology, Santa Cruz, CA).

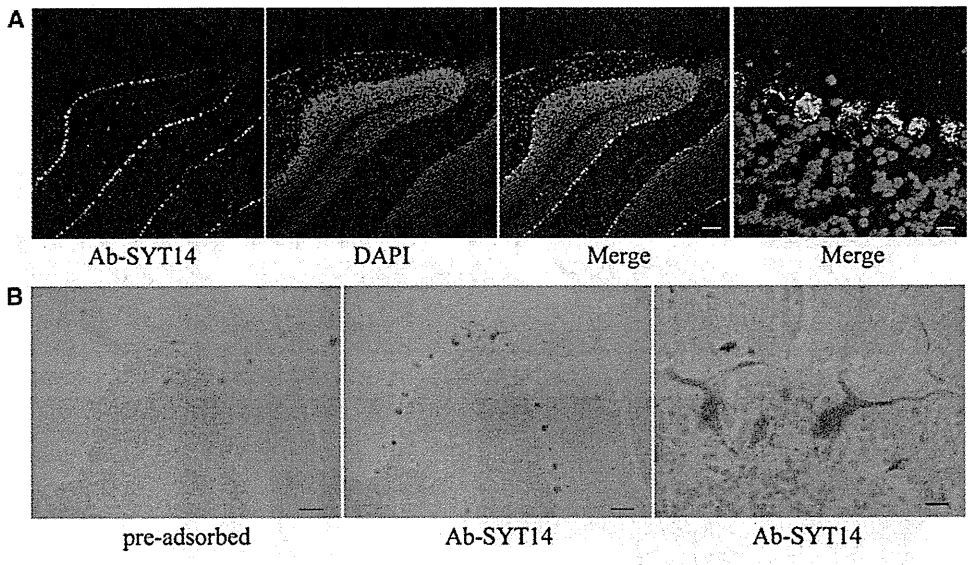

Figure 3. Selective Localization of SYT14 in Purkinje Cells of the Cerebellum in Mice and Humans
(A) Immunohistochemical analysis with the Ab-SYT14 antibody of the cerebellum from an adult mouse at 12 weeks of age. Nuclei were stained with DAPI (the scale bar represents 100 μm). A magnified image is shown in the first right panel (the scale bar represents 10 μm).The Ab-SYT14 antibody (0.9 mg/dl) was used at a dilution ration of 1:2000, and the Alexa-488-conjugated secondary antibody dilution was 1:1000.
(B) Immunohistochemical analysis with the Ab-SYT14 antibody of the cerebellum from the human control. Ab-SYT14 antibodies were preincubated with (left panel) or without (middle panel) peptide antigen before immunostaining. Nuclei were stained with hematoxylin (scale bars represent 100 μm). A magnified image is shown in the right panel (the scale bar represents 20 μm). The Ab-SYT14 antibody (0.9 mg/dl) was used at a dilution of 1:500.

performed with Ab-SYT14, as previously described.[19–21] Mouse brain sections were prepared at the RIKEN Brain Science Institute. Mouse experimental protocols were approved by the animal experiment committee of the RIKEN Brain Science Institute. The frozen brain of C57BL/6J mouse was mounted in Tissue-Tek and sliced to 10 μm sections with a freezing microtome. A human adult brain specimen was obtained through the postmortem examination of a brain from a control subject without neurodegenerative disorders. Informed consent was obtained from the family on the basis of the IRB-approved protocol of Yokohama City University School of Medicine. The human brain was fixed in 10% formalin and cut into 1-cm-thick slices. Sliced tissues were embedded in paraffin wax, and 5 μm sections were immunostained with primary antibodies and visualized with the Vectastain ABC kit (Vector Laboratories, Burlingame, CA). Selective localization of SYT14/Syt14 in Purkinje cells of the mouse cerebellum (Figure 3A) and human cerebellum (Figure 3B) were recognized, indicating that SYT14 plays an important role in the cerebellum. These data are in agreement with a scenario in which the *SYT14* mutation causes cerebellar degeneration in this family.

In this study, only one p.Gly484Asp mutation of *SYT14* was identified in association with SCA. Quintero-Rivera et al.[16] previously described a 12-year-old female with cerebral atrophy, absence seizures, developmental delay with a WISC III score of 58 for full IQ, and de novo t(1;3)(q32.1;q25.1) disrupting *SYT14*. Her brain MRI showed diffuse cerebral atrophy, including that of the cerebellar hemisphere and vermis. Although the inheritance modes are different (recessive impact on our family and dominant on the female patient), mild to moderate mental retardation and cerebellar atrophy are common among patients with *SYT14* abnormalities. It will be important to assess the future phenotype of the female patient studied by Quintero-Rivera et al.[16]

Relatively common ARCAs in Japan include ataxia, early-onset; oculomotor apraxia, hypoalbuminemia/ataxia-oculomotor apraxia 1 (EAOH/AOA1 [MIM 208920]); ataxia-oculomotor apraxia 2 (AOA2 [MIM 606002]); spastic ataxia; Charlevoix-Saguenay type (SACS [MIM 270550]); ataxia with isolated vitamin E deficiency (AVED [MIM 277460]); and ataxia-telangiectasia (AT [MIM 208900]). (Friedrich ataxia 1 [FRDA (MIM 229300)] has never been described in the Japanese population.) In this family, patients never showed ocularmotor apraxia, spasticity, peripheral neuropathy, retinal abnormality, immunological abnormality, or other systemic involvements. As an adult-onset type of pure ARCA, SYNE1-related ARCA (also known as spinocerebellar ataxia, autosomal-recessive 8; SCAR8 [MIM 610743]) is found to be caused by mutations of the gene encoding synaptic nuclear envelope protein 1.[22] Furthermore, these patients were not associated with psychomotor retardation. Thus, SYT14-mutated ARCA, described here, should be categorized to a distinct type of ARCA.

SYTs is a large family of transmembrane proteins associated with exocytosis of secretory vesicles (including synaptic vesicles).[23] The mammalian SYT family is composed

of 17 members. SYTs are anchored to the secretory vesicles via a single transmembrane domain (TM) close to its N terminus and have tandem cytoplasmic domains, C2A and C2B.[24] Among SYTs, SYT1 (MIM 185605) is involved in neurotransmitter release and has been intensively studied. The crystal structure of the C2 domains consists of a compact eight-stranded β-barrel with two protruding loops (loops 1 and 3) that form the Ca^{2+}-binding pockets.[25] SYT1 binds three and two Ca^{2+} ions via loops 1 and 3 of C2A and C2B, respectively. Ca^{2+} binding triggers the rapid penetration of the C2 domains into membranes harboring negatively charged phospholipids. Ca^{2+} also promotes SYT1 binding to t-SNAREs (target-membrane-soluble N-ethylmaleimide-sensitive factor attachment protein receptors). SYT1 is a key sensor for evoked and synchronous neurotransmitter release in many classes of neurons.[23] SYT14 also has TM, C2A, and C2B domains, but it has no conserved Ca^{2+}-binding motif that includes the conserved aspartic acid residues in loops 1 and 3 of C2A and C2B.[26] Although the roles of SYTs as Ca^{2+} sensors have been studied extensively, little is known about Ca^{2+}-independent SYTs, which might inhibit the SNARE-catalyzed fusion in both the absence and presence of Ca^{2+}.[27] Recently, Zhang et al.[28] suggested that Ca^{2+}-independent SYT4 (MIM 600103) negatively regulates exocytosis, regardless of its inability to induce Ca^{2+}-dependent exocytosis.

SYT14 has phospholipid-binding activity that is Ca^{2+} independent.[14] The glycine residue mutated in the family is located around the C2B domain loop 1, which plays an important role in binding to phospholipids in SYT1.[25] We confirmed that, compared to the wild-type, the mutation did not alter the binding activity of SYT14 to phospholipids. In an overexpression system, wild-type SYT14 as well as normal variants were distributed in the cytoplasm close to the plasma membrane, showing in-line accumulation along with the membrane. In contrast, the p.Gly484Asp mutant showed a different (reticular) distribution pattern. In the ER, several cotranslational and posttranslational modifications that are required for the correct folding of transmembrane and secretory proteins take place.[29,30] Incompletely folded proteins are generally excluded from ER exit sites.[29] The fact that the p.Gly484Asp was not properly transferred from the ER suggests that the mutant protein might not fold correctly. The lower yield of the mutant protein as compared to the wild-type in the bacterial expression system we performed also supports the improper folding of the mutant. Abnormal distribution in the ER might result in the loss of function of SYT14 or in ER dysfunction.

In conclusion we have shown that SYT14 is localized specifically in Purkinje cells of mouse and human cerebellum. The results strongly support the involvement of SYT14 in the pathogenesis of SCA and are consistent with the atrophy of the cerebellum seen in both patients. A possible relationship between SYTs and neurodegeneration has been suggested previously,[31] and here we provide data that support the idea that disruption of an SYT protein is involved in human neurodegeneration and that exocytosis machinery can be involved in one of the pathomechanisms of neurodegeneration.

Supplemental Data

Supplemental Data include two figures and five tables and can be found with this article online at http://www.cell.com/AJHG/.

Acknowledgments

We would like to thank the patients and their family for their participation in this study. We are indebted to Syu-ichi Hirai (Department of Molecular Biology, Yokohama City University) for providing useful technical information about subcellular fractionation and to Keiko Yamaoka (Kanagawa Rehabilitation Center) for providing brain tissue from the control subject. This work was supported by research grants from the Ministry of Health, Labour, and Welfare (H.S., N. Miyake, and N. Matsumoto), the Japan Science and Technology Agency (N. Matsumoto), a Grant-in-Aid for Scientific Research from the Japan Society for the Promotion of Science (N. Matsumoto), a Grant-in-Aid for Young Scientist from the Japan Society for the Promotion of Science (H.D., N. Miyake, and H.S.) and a grant-in-aid from The Kimi Imai Memorial Foundation for Research of Incurable Neuromuscular Diseases (H.D.).

Received: June 4, 2011
Revised: July 11, 2011
Accepted: July 15, 2011
Published online: August 11, 2011

Web Resources

The URLs for data presented herein are as follows:

Align GVGD, http://agvgd.iarc.fr/
Allen Human brain Atlas, http://human.brain-map.org/
Allen Mouse Brain Atlas, http://mouse.brain-map.org/
HomozygosityMapper, http://www.homozygositymapper.org/
Online Mendelian Inheritance in Man (OMIM), http://www.omim.org/
PolyPhen, http://genetics.bwh.harvard.edu/pph/
PolyPhen2, http://genetics.bwh.harvard.edu/pph2/
SIFT, http://blocks.fhcrc.org/sift/SIFT.html

Rerefences

1. Fogel, B.L., and Perlman, S. (2007). Clinical features and molecular genetics of autosomal recessive cerebellar ataxias. Lancet Neurol. *6*, 245–257.
2. Palau, F., and Espinós, C. (2006). Autosomal recessive cerebellar ataxias. Orphanet J. Rare Dis. *1*, 47.
3. Embiruçu, E.K., Martyn, M.L., Schlesinger, D., and Kok, F. (2009). Autosomal recessive ataxias: 20 types, and counting. Arq. Neuropsiquiatr. *67*, 1143–1156.
4. Anheim, M., Fleury, M., Monga, B., Laugel, V., Chaigne, D., Rodier, G., Ginglinger, E., Boulay, C., Courtois, S., Drouot, N., et al. (2010). Epidemiological, clinical, paraclinical and

molecular study of a cohort of 102 patients affected with autosomal recessive progressive cerebellar ataxia from Alsace, Eastern France: Implications for clinical management. Neurogenetics *11*, 1–12.
5. Manto, M., and Marmolino, D. (2009). Cerebellar ataxias. Curr. Opin. Neurol. *22*, 419–429.
6. Vermeer, S., Hoischen, A., Meijer, R.P., Gilissen, C., Neveling, K., Wieskamp, N., de Brouwer, A., Koenig, M., Anheim, M., Assoum, M., et al. (2010). Targeted next-generation sequencing of a 12.5 Mb homozygous region reveals *ANO10* mutations in patients with autosomal-recessive cerebellar ataxia. Am. J. Hum. Genet. *87*, 813–819.
7. Seelow, D., Schuelke, M., Hildebrandt, F., and Nurnberg, P. (2009). HomozygosityMapper—An interactive approach to homozygosity mapping. Nucleic Acids Res. *37*, W593–W599.
8. Bahlo, M., and Bromhead, C.J. (2009). Generating linkage mapping files from Affymetrix SNP chip data. Bioinformatics *25*, 1961–1962.
9. Gudbjartsson, D.F., Thorvaldsson, T., Kong, A., Gunnarsson, G., and Ingolfsdottir, A. (2005). Allegro version 2. Nat. Genet. *37*, 1015–1016.
10. Li, H., Ruan, J., and Durbin, R. (2008). Mapping short DNA sequencing reads and calling variants using mapping quality scores. Genome Res. *18*, 1851–1858.
11. Gilissen, C., Arts, H.H., Hoischen, A., Spruijt, L., Mans, D.A., Arts, P., van Lier, B., Steehouwer, M., van Reeuwijk, J., Kant, S.G., et al. (2010). Exome sequencing identifies *WDR35* variants involved in Sensenbrenner syndrome. Am. J. Hum. Genet. *87*, 418–423.
12. Tsurusaki, Y., Osaka, H., Hamanoue, H., Shimbo, H., Tsuji, M., Doi, H., Saitsu, H., Matsumoto, N., and Miyake, N. (2011). Rapid detection of a mutation causing X-linked leucoencephalopathy by exome sequencing. J. Med. Genet., in press. Published online March 17, 2011. 10.1136/jmg.2010.083535.
13. Becker, J., Semler, O., Gilissen, C., Li, Y., Bolz, H.J., Giunta, C., Bergmann, C., Rohrbach, M., Koerber, F., Zimmermann, K., et al. (2011). Exome sequencing identifies truncating mutations in human *SERPINF1* in autosomal-recessive osteogenesis imperfecta. Am. J. Hum. Genet. *88*, 362–371.
14. Fukuda, M. (2003). Molecular cloning, expression, and characterization of a novel class of synaptotagmin (Syt XIV) conserved from *Drosophila* to humans. J. Biochem. *133*, 641–649.
15. Adolfsen, B., Saraswati, S., Yoshihara, M., and Littleton, J.T. (2004). Synaptotagmins are trafficked to distinct subcellular domains including the postsynaptic compartment. J. Cell Biol. *166*, 249–260.
16. Quintero-Rivera, F., Chan, A., Donovan, D.J., Gusella, J.F., and Ligon, A.H. (2007). Disruption of a synaptotagmin (*SYT14*) associated with neurodevelopmental abnormalities. Am. J. Med. Genet. A. *143*, 558–563.
17. Michelsen, U., and von Hagen, J. (2009). Isolation of subcellular organelles and structures. Methods Enzymol. *463*, 305–328.
18. Fukuda, M., Kojima, T., and Mikoshiba, K. (1996). Phospholipid composition dependence of Ca^{2+}-dependent phospholipid binding to the C2A domain of synaptotagmin IV. J. Biol. Chem. *271*, 8430–8434.
19. Doi, H., Mitsui, K., Kurosawa, M., Machida, Y., Kuroiwa, Y., and Nukina, N. (2004). Identification of ubiquitin-interacting proteins in purified polyglutamine aggregates. FEBS Lett. *571*, 171–176.
20. Jana, N.R., Tanaka, M., Wang, G., and Nukina, N. (2000). Polyglutamine length-dependent interaction of Hsp40 and Hsp70 family chaperones with truncated N-terminal huntingtin: Their role in suppression of aggregation and cellular toxicity. Hum. Mol. Genet. *9*, 2009–2018.
21. Oyama, F., Miyazaki, H., Sakamoto, N., Becquet, C., Machida, Y., Kaneko, K., Uchikawa, C., Suzuki, T., Kurosawa, M., Ikeda, T., et al. (2006). Sodium channel beta4 subunit: down-regulation and possible involvement in neuritic degeneration in Huntington's disease transgenic mice. J. Neurochem. *98*, 518–529.
22. Gros-Louis, F., Dupré, N., Dion, P., Fox, M.A., Laurent, S., Verreault, S., Sanes, J.R., Bouchard, J.P., and Rouleau, G.A. (2007). Mutations in *SYNE1* lead to a newly discovered form of autosomal recessive cerebellar ataxia. Nat. Genet. *39*, 80–85.
23. McCue, H.V., Haynes, L.P., and Burgoyne, R.D. (2010). The diversity of calcium sensor proteins in the regulation of neuronal function. Cold Spring Harb. Perspect. Biol. *2*, a004085.
24. Bai, J., and Chapman, E.R. (2004). The C2 domains of synaptotagmin—partners in exocytosis. Trends Biochem. Sci. *29*, 143–151.
25. Chapman, E.R. (2008). How does synaptotagmin trigger neurotransmitter release? Annu. Rev. Biochem. *77*, 615–641.
26. Rickman, C., Craxton, M., Osborne, S., and Davletov, B. (2004). Comparative analysis of tandem C2 domains from the mammalian synaptotagmin family. Biochem. J. *378*, 681–686.
27. Bhalla, A., Chicka, M.C., and Chapman, E.R. (2008). Analysis of the synaptotagmin family during reconstituted membrane fusion. Uncovering a class of inhibitory isoforms. J. Biol. Chem. *283*, 21799–21807.
28. Zhang, G., Bai, H., Zhang, H., Dean, C., Wu, Q., Li, J., Guariglia, S., Meng, Q., and Cai, D. (2011). Neuropeptide exocytosis involving synaptotagmin-4 and oxytocin in hypothalamic programming of body weight and energy balance. Neuron *69*, 523–535.
29. Ellgaard, L., and Helenius, A. (2003). Quality control in the endoplasmic reticulum. Nat. Rev. Mol. Cell Biol. *4*, 181–191.
30. Colgan, S.M., Hashimi, A.A., and Austin, R.C. (2011). Endoplasmic reticulum stress and lipid dysregulation. Expert Rev. Mol. Med. *13*, e4.
31. Glavan, G., Schliebs, R., and Zivin, M. (2009). Synaptotagmins in neurodegeneration. Anat. Rec. (Hoboken) *292*, 1849–1862.
32. Schmitz-Hübsch, T., du Montcel, S.T., Baliko, L., Berciano, J., Boesch, S., Depondt, C., Giunti, P., Globas, C., Infante, J., Kang, J.S., et al. (2006). Scale for the assessment and rating of ataxia: Development of a new clinical scale. Neurology *66*, 1717–1720.

REPORT

Mutations in *POLR3A* and *POLR3B* Encoding RNA Polymerase III Subunits Cause an Autosomal-Recessive Hypomyelinating Leukoencephalopathy

Hirotomo Saitsu,[1,*] Hitoshi Osaka,[2] Masayuki Sasaki,[3] Jun-ichi Takanashi,[4] Keisuke Hamada,[5] Akio Yamashita,[6] Hidehiro Shibayama,[7] Masaaki Shiina,[5] Yukiko Kondo,[1] Kiyomi Nishiyama,[1] Yoshinori Tsurusaki,[1] Noriko Miyake,[1] Hiroshi Doi,[1] Kazuhiro Ogata,[5] Ken Inoue,[8] and Naomichi Matsumoto[1,*]

Congenital hypomyelinating disorders are a heterogeneous group of inherited leukoencephalopathies characterized by abnormal myelin formation. We have recently reported a hypomyelinating syndrome characterized by diffuse cerebral hypomyelination with cerebellar atrophy and hypoplasia of the corpus callosum (HCAHC). We performed whole-exome sequencing of three unrelated individuals with HCAHC and identified compound heterozygous mutations in *POLR3B* in two individuals. The mutations include a nonsense mutation, a splice-site mutation, and two missense mutations at evolutionally conserved amino acids. Using reverse transcription-PCR and sequencing, we demonstrated that the splice-site mutation caused deletion of exon 18 from *POLR3B* mRNA and that the transcript harboring the nonsense mutation underwent nonsense-mediated mRNA decay. We also identified compound heterozygous missense mutations in *POLR3A* in the remaining individual. *POLR3A* and *POLR3B* encode the largest and second largest subunits of RNA Polymerase III (Pol III), RPC1 and RPC2, respectively. RPC1 and RPC2 together form the active center of the polymerase and contribute to the catalytic activity of the polymerase. Pol III is involved in the transcription of small noncoding RNAs, such as 5S ribosomal RNA and all transfer RNAs (tRNA). We hypothesize that perturbation of Pol III target transcription, especially of tRNAs, could be a common pathological mechanism underlying *POLR3A* and *POLR3B* mutations.

Congenital hypomyelinating disorders form a heterogeneous group of central nervous system leukoencephalopathies that is characterized by abnormal myelin formation. Although these conditions are readily recognized by brain magnetic resonance imaging (MRI), many cases are not diagnosed correctly.[1] Several syndromes affecting myelination, such as hypomyelination with hypodontia and hypogonadotropic hypogonadism (4H) syndrome (MIM 612440) and hypomyelination with atrophy of the basal ganglia and cerebellum (H-ABC) (MIM 612438), have been described.[2–5] We have recently reported a hypomyelinating syndrome characterized by diffuse cerebral hypomyelination with cerebellar atrophy and hypoplasia of the corpus callosum (HCAHC).[6] Individuals with HCAHC do not show hypodontia or atrophy of the basal ganglia, which are observed in 4H syndrome and H-ABC; however, diffuse hypomyelination, atrophy, or hypoplasia of the cerebellum and corpus callosum are overlapping features of these three syndromes, suggesting that there might be a common underlying pathological mechanism.

Here, we report on four individuals with HCAHC from three unrelated families (Figure 1A; Table 1). Clinical information and peripheral blood or saliva samples were obtained from the family members after obtaining written informed consent. Experimental protocols were approved by the Institutional Review Board of Yokohama City University. To identify pathogenic mutations, we performed whole-exome sequencing of three probands from three unrelated families (individuals 1, 3, and 4). DNAs were captured with the SureSelect Human All Exon 50Mb Kit (Agilent Technologies, Santa Clara, CA) and sequenced with one lane per sample on an Illumina GAIIx (Illumina, San Diego, CA) with 108 bp paired-end reads. Image analysis and base calling were performed by sequence control software real-time analysis and CASAVA software v1.7 (Illumina). A total of 90,014,368 (individual 1), 86,942,264 (individual 3), and 92,168,758 (individual 4) paired-end reads were obtained and aligned to the human reference genome sequence (GRCh37/hg19) with MAQ[7] and NextGENe software v2.00 with sequence condensation by consolidation (SoftGenetics, State College, PA). This approach resulted in more than 88% of target exomes being covered by ten reads or more (see Table S1, available online). Single nucleotide variants (SNVs) were called with MAQ and NextGENe. Small insertions and deletions were

[1]Department of Human Genetics, Yokohama City University Graduate School of Medicine, 3-9 Fukuura, Kanazawa-ku, Yokohama 236-0004, Japan; [2]Division of Neurology, Clinical Research Institute, Kanagawa Children's Medical Center, 2-138-4 Mutsukawa, Minami-ku, Yokohama 232-8555, Japan; [3]Department of Child Neurology, National Center of Neurology and Psychiatry, 4-1-1 Ogawahigashi-cho Kodaira, Tokyo 187-8551, Japan; [4]Department of Pediatrics, Kameda Medical Center, 929 Higashi-cho, Kamogawa-shi, Chiba 296-8602, Japan; [5]Department of Biochemistry, Yokohama City University Graduate School of Medicine, 3-9 Fukuura, Kanazawa-ku, Yokohama 236-0004, Japan; [6]Department of Molecular Biology, Yokohama City University Graduate School of Medicine, 3-9 Fukuura, Kanazawa-ku, Yokohama 236-0004, Japan; [7]Department of Neurology, Kameda Medical Center, 929 Higashi-cho, Kamogawa-shi, Chiba 296-8602, Japan; [8]Department of Mental Retardation and Birth Defect Research, National Institute of Neuroscience, National Center of Neurology and Psychiatry, 4-1-1 Ogawahigashi-cho Kodaira, Tokyo 187-8551, Japan
*Correspondence: hsaitsu@yokohama-cu.ac.jp (H.S.), naomat@yokohama-cu.ac.jp (N.M.)
DOI 10.1016/j.ajhg.2011.10.003. ©2011 by The American Society of Human Genetics. All rights reserved.

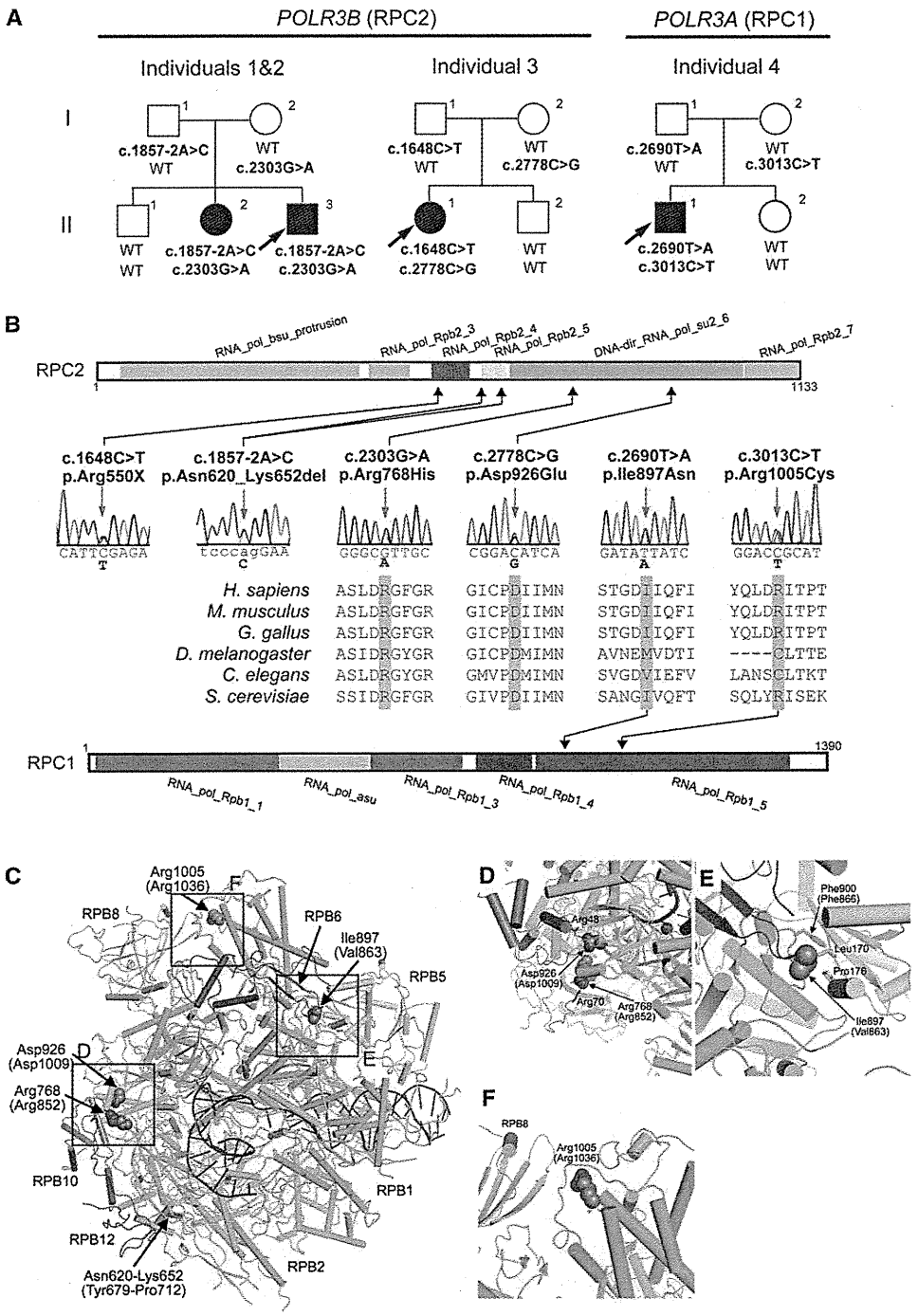

Figure 1. Mutations in *POLR3B* and *POLR3A*

(A) Pedigrees of four kindreds with HCAHC are shown. We identified four mutations in *POLR3B* encoding RPC2 in three individuals from two unrelated families and two mutations in *POLR3A* encoding RPC1 in one family. The segregation of each mutation is shown.

(B) Schematic representation of RPC2 (upper) and RPC1 (lower) proteins with Pfam domains (from Ensembl). Locations of each amino-acid-altering mutation are depicted with electropherograms. All of the missense mutations occurred at evolutionally conserved amino acids. Homologous sequences were aligned with the CLUSTALW website.

(C–F) 3D representations of RPC1 and RPC2 mutations. Mutated amino acids in RPC1 and RPC2 are shown along with their equivalent positions in the homologous RPB1 and RPB2 subunits of RNA Polymerase II (amino acid and its position in parenthesis). The structure and positions of mutations are illustrated by PyMOL with the crystal structure (PDB accession number 3GTP). RPB3, RPB9, and RPB11 subunits, which are specific to RNA Polymerase II, have been omitted from the figure. RPB1 is shown in green, RPB2 in sky blue, RPB5 in yellow, RPB6 in dark blue, RPB8 in pink, RPB10 in orange, RPB12 in purple, DNA in brown, and RNA in red. Amino acids that interact with mutated amino acids are also shown.